RESEARCH PAPER

Small Genome vs. Complex Retrovirus: Theoretical Considerations of Influenza A and HIV-1 Replication and Therapeutic Exploitation

Saken Khaidarov[1], Aizhan Beisenova[1*], Bayan Nurgalieva[2*], Symbat Yerkhanova[1], Venera Israilova[3], Nazima Zarubekova[4]

[1] Department of Molecular Biology and Medical Genetics, Kazakh National Medical University Named After S.D. Asfendiyarov, Zheltoksan 37A Street, Almaty 050012, Kazakhstan

[2] Department of Propaedeutics of Internal Medicine, Kazakh National Medical University Named After S.D. Asfendiyarov, Tole-bi Street 94, Almaty 050012, Kazakhstan

[3] University of International Business, Faculty of Medicine. City Cardiology Center, Abay ave. 8A, Almaty 050010, Kazakhstan

[4] Department of Emergency and Urgent Medical Care, Kazakh National Medical University Named After S.D. Asfendiyarov, Tole-bi Street 94, Almaty 050012, Kazakhstan

[*] **Corresponding Authors:** Aizhan Beisenova, Bayan Nurgalieva

Received: 17th Mar, 2026 | Revised: 29th Mar, 2026 | Accepted: 19th Apr, 2026 | Available Online: 5th May, 2026

ABSTRACT

Influenza A virus (IAV) remains a significant global health threat due to its rapid mutation rate, seasonal epidemics, and pandemic potential. Continuous viral evolution and emerging resistance to existing antivirals necessitate the evaluation of alternative or repurposed antiviral strategies. Tenofovir alafenamide (TAF), a phosphonamidite pro-drug of tenofovir primarily used in antiretroviral therapy, has demonstrated intracellular stability and a favorable safety profile. In this study, we investigated the time- and concentration-dependent antiviral activity and cytotoxicity of TAF in Influenza A–infected cell culture over a 120-h period. Antiviral efficacy was quantified as percentage inhibition of viral replication, while cytotoxicity was assessed using the MTT assay to determine cell viability. TAF exhibited progressive, exposure-dependent suppression of Influenza A replication, with inhibition exceeding 80% at higher concentrations after prolonged incubation. Importantly, host cell viability remained ≥70% under corresponding conditions, and the CC_{50} was not reached within the tested concentration range. The estimated EC_{50} values indicated significant antiviral activity with a favourable selectivity window. These findings suggest that TAF exerts time-dependent inhibitory effects on Influenza A virus while preserving cellular viability, supporting further investigation of nucleotide-analogue–based strategies for RNA virus replication control.

Keywords: Genome size; Viral competition; Sars-cov-2; Newcastle disease virus; Influenza a; Hpv-1; Coinfection.

How to cite this article: Khaidarov S, Beisenova A, Nurgalieva B, Yerkhanova S, Israilova V, Zarubekova N. Small Genome vs. Complex Retrovirus: Theoretical Considerations of Influenza A and HIV-1 Replication and Therapeutic Exploitation. Int J Drug Deliv Technol. 2026;16(5): 646-677. DOI: 10.25258/ijddt.16.5.71

Source of support: Nil.

Conflict of interest: None

1. Introduction

1.1. Genome matters

Viruses display extraordinary diversity in genome size, from 3–5 kb paramyxoviruses to >30 kb coronaviruses and >8 kb papillomaviruses. Genome size shapes coding capacity, replication strategy, evolutionary flexibility, and immune evasion. Coinfections—common in natural hosts—create ecological arenas in which viral genomes compete for cellular resources, metabolic pathways, and immune space. Small-genome viruses often outpace larger viruses early in infection through streamlined replication, whereas large-genome viruses counterbalance this by producing complex immunomodulatory proteins, reprogramming host cells, and persisting. Here, we synthesise evidence from NDV biology, IAV zoonotic transmission, SARS-CoV-2 replication and antiviral sensitivity, and HPV-1 cell-cycle manipulation to propose

genome size as a key variable governing viral dominance.

The depicted trend (Figure 1) illustrates a fundamental life-history trade-off in virology. Viruses with compact genomes (e.g., 3–15 kb) are constrained in their genetic coding capacity, which often selects for strategies centred on rapid replication and high progeny output ("r-strategy") to outpace host defences [1]. For instance, Influenza A Virus (IAV), with its segmented ~13.5 kb RNA genome, accomplishes a replication cycle within 6–8 hours, facilitating swift spread [2].

Conversely, large-genome viruses (e.g., >25 kb) possess the genetic repertoire to encode sophisticated tools for modulating the host cell environment and evading immune responses ("K-strategy"). This includes proteins that interfere with interferon signalling, apoptosis, and antigen presentation. The ~30 kb SARS-CoV-2 genome, for example, encodes multiple accessory proteins (e.g., ORF3a, ORF6, ORF7a, ORF8) that antagonise innate immune pathways, contributing to a more protracted and regulated replication cycle [3]. Similarly, large DNA viruses such as poxviruses (~200 kb) encode numerous immunomodulators, consistent with their slower, persistent replication strategy [4]. This dichotomy underscores how genome size is a key determinant of viral replication dynamics and host interaction complexity.

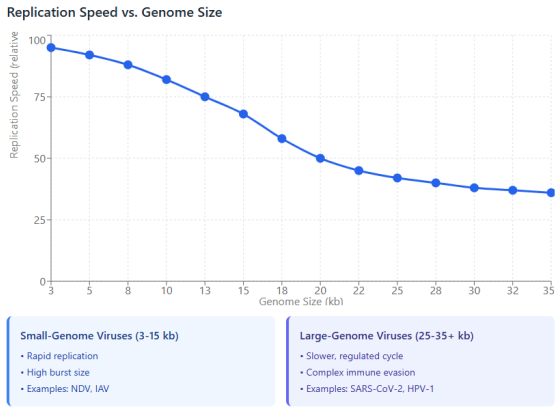

Figure 1. The inverse relationship between viral genome size and relative replication speed. Viruses with small genomes (e.g., *Paramyxoviridae* like NDV, *Orthomyxoviridae* like IAV) typically exhibit rapid replication cycles and high burst sizes. In contrast, viruses with large genomes (e.g., *Coronaviridae* such as SARS-CoV-2, Papillomaviridae such as HPV-1) generally undergo slower, more regulated replication cycles, often involving complex mechanisms for immune evasion and host interactions. The figure is based on generalised trends in viral life-history strategies.

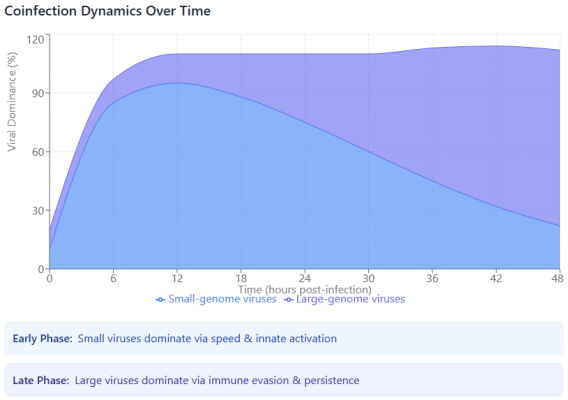

Figure 2. Hypothetical model of shifting viral dominance during coinfection over time. In the early phase, viruses with small genomes and rapid replication cycles (e.g., Influenza A Virus - IAV) often achieve initial dominance by exploiting speed and inducing a potent but frequently nonspecific innate immune response. In the late phase, viruses with larger genomes and complex immune-evasion strategies (e.g., SARS-CoV-2) may gain dominance by resisting activated host defences and establishing persistent infection. The model illustrates a temporal trade-off based on distinct viral life-history strategies [5,6].

This model conceptualises a dynamic and competitive landscape during viral coinfection, in which dominance shifts according to the temporal alignment of each virus's strategic advantages [5]. During the early phase, small-genome, fast-replicating viruses (e.g., Influenza A Virus, Respiratory Syncytial Virus) can quickly hijack cellular machinery and produce a large burst of progeny. Furthermore, their infection often triggers a robust type I interferon (IFN) response [7]. While this IFN response is an antiviral defence, it can simultaneously create an environment that temporarily suppresses the replication of a co-infecting virus, a phenomenon known as viral interference, thereby cementing the initial dominance of the first virus [8].

However, this early innate immune activation sets the stage for the late phase. Large-genome viruses (e.g., SARS-CoV-2, human cytomegalovirus) frequently encode numerous proteins dedicated to antagonising

host immune pathways, including IFN signalling, antigen presentation, and apoptosis [9,10]. For instance, SARS-CoV-2 proteins like ORF6 and NSP1 efficiently block IFN production and signalling [10]. Consequently, these viruses are better equipped to tolerate or suppress the already-activated host defence state. Their slower, more regulated replication cycle favours persistence, allowing them to outlast the acute phase of the fast-replicating virus and potentially become the dominant pathogen later in the infection. This biphasic dynamic has significant implications for disease severity, transmission, and therapeutic intervention during coinfections.

1.2. Viral Genome Size and Replication Strategy

1. 2.1. Small-genome RNA viruses: speed over complexity

Newcastle disease virus (NDV) contains a ~15.2 kb negative-sense RNA genome encoding only seven structural proteins, yet it replicates efficiently in epithelial tissues and induces a strong innate immune response. Its polymerase follows a stop–start transcription gradient, enabling rapid but less regulated replication cycles, as described in studies on NDV molecular and vector biology [11].

Similarly, Influenza A virus (IAV) carries eight RNA segments totalling ~13.5 kb and leverages segmented reassortment to accelerate evolutionary adaptation and host switching, as shown in ecological and zoonotic analyses of influenza circulation in wild birds and mammals [4].

Both NDV and IAV rely on high mutation rates, fast replication, and high burst sizes, which confer competitive advantages during acute infection.

1.2.2. Large-genome viruses: immune modulation and persistence

SARS-CoV-2 (~30 kb) encodes more than 25 proteins, including multiple innate-immune antagonists (e.g., ORF6, ORF8). These allow it to dampen antiviral signalling, sustain replication, and establish prolonged infection cycles. Antiviral studies demonstrate that SARS-CoV-2 replication is strongly suppressed only under high pharmacological pressure (e.g., TDF/TAF treatment), with dose-dependent inhibition observed in vitro [3].

HPV-1 (~8 kb dsDNA) encodes E6/E7 oncoproteins that manipulate p53 and Rb pathways, enabling long-term persistence and immune evasion. These mechanisms influence competitive behaviour during coinfection by altering epithelial turnover and weakening antiviral responses [2].

1.3. Competitive Dynamics in Coinfection

1.3.1. Small-genome viruses dominate early replication

Rapid RNA virus replication can suppress slower viruses through:

- Resource monopolisation (ribosomes, nucleotides)
- Superinfection exclusion mediated by early interferon bursts
- Cytopathic effects that reduce available host cells

NDV's intense innate immune stimulation and fast cytoplasmic replication can significantly restrict other viruses, consistent with NDV vaccine-vector studies demonstrating impaired replication of co-introduced viral antigens [10].

IAV's rapid replication has likewise been shown to outcompete slower viruses in avian and mammalian hosts, driven by high mutation rates, rapid polymerase activity, and efficient respiratory tract infection [4].

1.3.2. Large-genome viruses dominate long-term infection niches

Large-genome viruses employ complex accessory proteins that:

- Suppress interferon signaling (SARS-CoV-2 ORF6/ORF7)
- Manipulate cell-cycle progression (HPV E6/E7)
- Rewire metabolic and transcriptional pathways
- Persist in immune-privileged or immune-suppressed environments

SARS-CoV-2's expanded immune-modulatory repertoire enhances competitive persistence during coinfection, especially when acute viruses trigger inflammatory responses that inadvertently promote coronavirus survival. TDF/TAF antiviral studies further highlight the virus's resilience, requiring high concentrations or prolonged treatment for suppression [3].

HPV-mediated persistence, supported by control of the cell cycle and evasion of innate immune responses, establishes long-lived epithelial niches in which rapid RNA viruses cannot sustain replication.

1.4. Case Analyses: Comparative Virus–Virus Interactions

1.4.1. NDV vs. SARS-CoV-2

NDV's streamlined genome supports rapid replication and strong interferon induction, whereas

SARS-CoV-2 possesses extensive immune-evasion machinery, including inhibition of IRF3 and STAT1, giving it dominance in longer-term infections. NDV nonetheless remains a predictable and stable vaccine vector with minimal genomic interference [10].

1.4.2. Influenza A vs coronaviruses in the respiratory tract

IAV's segmented genome enables rapid host adaptation and zoonotic emergence. In coinfected individuals, IAV often peaks earlier due to rapid replication, whereas SARS-CoV-2 typically persists longer due to robust immunomodulatory activity. These dynamics reflect how genome architecture influences competitive advantage in respiratory tissues [4].

1.4.3. HPV-1 vs acute RNA viruses

HPV-1 depends on epithelial differentiation and employs persistent replication strategies with minimal cytopathic effect. During coinfection, HPV avoids direct competition while indirectly benefiting from epithelial inflammation caused by acute RNA viruses.

1.5. Genome Size as a Predictor of Immune Evasion and Evolution

1.5.1. Small genomes evolve rapidly

Error-prone RNA polymerases allow small RNA viruses—such as NDV and IAV—to accumulate mutations, enabling them to quickly:

- Rapid host adaptation
- Efficient immune escape
- Reassortment (in the case of IAV)

This accelerates competitive displacement during short infection windows.

1.5.2. Large genomes deploy multifunctional immune-modulation systems

Large-genome viruses encode:

- Interferon antagonists
- Chemokine/immune mimics
- Accessory proteins that alter host metabolism
- Mechanisms for long-term persistence

SARS-CoV-2 exemplifies this complexity. Antiviral assays demonstrate that suppression of replication requires substantial pharmacological pressure, indicating a strong baseline immune-evasion capacity [3].

1.6. Implications for Viral Pathogenesis and Evolution

1.6.1. Viral interference as a natural selective force

Coinfection pressures select for:

- High replication speed in small-genome viruses
- Strong immune-modulation in large-genome viruses
- Niche partitioning across tissues or infection stages

1.6.2. Public health significance

Understanding genome-size-driven viral behaviour informs:

- Predictive models of seasonal dominance
- Surveillance of zoonotic emergence (exemplified by avian-origin IAV dynamics [4])
- Vaccine interference and vector design (using NDV-based platforms [10])

1.6.3. Therapeutic exploitation

Fast-replicating viruses may suppress persistent pathogens through competitive exclusion or immune activation. NDV is being explored as an oncolytic virus capable of overwhelming tumour-modified antiviral defences [10].

1.7 Viruses

1. 7.1. *Human Papillomaviruses: Minimal Genomes, Maximal Specificity, and Limited Functional Relevance*

Genome Architecture and Biological Minimalism

Human papillomaviruses (HPVs) are small, non-enveloped double-stranded DNA viruses with circular genomes of approximately 7.9–8.1 kb, placing them among the most genomically constrained DNA viruses infecting humans [11,12]. The genome encodes a minimal set of early (E1–E7) and late (L1, L2) proteins, with no accessory genes dedicated to immune modulation, metabolic reprogramming, or replication autonomy [1]. This architectural simplicity enforces an obligate dependence on host-cell DNA polymerases and epithelial differentiation programs, resulting in slow, tightly regulated replication kinetics [12].

Unlike larger DNA viruses, HPVs lack the genetic capacity to manipulate innate immune signalling or antiviral restriction pathways actively. Their replication strategy is therefore not competitive but parasitic in the strictest sense—passively exploiting host cell-cycle transitions with minimal perturbation of cellular homeostasis [11]. From a genome-size perspective, HPV represents an extreme endpoint of viral minimalism, where compactness directly limits functional versatility.

Extreme Host and Tissue Specificity

HPVs display exceptional host and tissue specificity, infecting only stratified squamous epithelia of skin or mucosa, with individual genotypes restricted to narrow anatomical niches [12]. Viral entry, genome maintenance, and productive replication are inseparably linked to keratinocyte differentiation, a constraint that sharply limits tropism expansion and adaptive flexibility [3].

This specificity contributes to immune invisibility rather than immune evasion: HPV avoids immune detection largely by failing to trigger danger signals, inflammatory cascades, or cytolytic damage [13]. In competitive or coinfected environments, such biological restraint renders HPV largely irrelevant—it neither interferes with nor suppresses other viruses, nor does it adapt rapidly to altered host conditions.

Relative Harmlessness and Low Acute Pathogenicity

In the majority of immunocompetent individuals, HPV infection is asymptomatic and transient, with spontaneous clearance occurring without systemic immune activation [3]. Acute pathogenicity is virtually absent, as the viral life cycle is non-lytic and produces negligible tissue damage. Even for oncogenic HPV types, disease manifestations arise indirectly through long-term expression of E6 and E7 proteins, which dysregulate p53 and retinoblastoma pathways rather than inducing direct cytopathic effects [14].

Importantly, this oncogenic potential does not contradict HPV's overall biological mildness. Malignancy is a statistical consequence of persistence, not virulence. Compared with RNA viruses or large DNA viruses, HPVs lack both the capacity to drive acute disease and a competitive replication advantage.

Limited Utility in Modern Biotechnology

Despite extensive molecular characterisation, HPVs have contributed minimally to modern virology and biotechnology beyond serving as sources of structural antigens for prophylactic vaccines. Their limitations are inherent and non-negotiable:

- Viral vector applications are precluded by extremely limited genome capacity, which cannot tolerate insertion of foreign genetic material [12].
- Oncolytic or therapeutic uses are implausible due to slow, differentiation-dependent, non-lytic replication [14].
- Antiviral research relevance is marginal, as HPVs lack viral polymerases, proofreading mechanisms, or error-prone replication dynamics that are central to antiviral drug targeting or lethal mutagenesis strategies [1,15].

Thus, while biologically elegant, HPVs are functionally inert from an applied virology standpoint—well-studied, well-mapped, and largely unusable.

HPV within Genome Size–Driven Viral Competition

When viewed through the lens of genome-size-driven viral competition, HPV occupies a biologically passive niche. Its small genome enforces low replication speed, absence of immune antagonism, and strict ecological confinement [1,15]. During coinfections, HPV neither competes for resources nor meaningfully alters the host antiviral environment. Instead, it persists orthogonally to acute viral dynamics dominated by fast-replicating RNA viruses or large-genome DNA viruses equipped with immune-modulatory arsenals.

In this framework, HPV is not a competitor but a bystander—evolutionarily stable, biologically quiet, and competitively negligible.

Human papillomaviruses exemplify how extreme genome reduction trades biological influence for persistence. Their small genome ensures specificity, stability, and long-term survival, but at the cost of adaptability, competitiveness, and technological relevance. In the context of viral genome size, HPV represents the lower functional boundary: a virus that survives not by doing more, but by doing almost nothing—remarkably well.

1.7.2 Newcastle Disease Virus: A Small Genome Optimised for Speed, Interference, and Biotechnological Utility

Genome Architecture and Functional Economy

Newcastle disease virus (NDV), a member of the *family Paramyxoviridae, possesses a single-stranded,* negative-sense RNA genome of approximately 15.2 kb. This genome encodes only six structural proteins (N, P, M, F, HN, L) and two non-structural proteins generated by RNA editing (V and W), placing NDV firmly among small-genome RNA viruses [16,17]. Despite this limited coding capacity, NDV exhibits remarkable replication efficiency and functional impact.

The compact NDV genome enforces a strict transcriptional hierarchy and rapid replication

kinetics. Viral RNA synthesis occurs entirely in the cytoplasm, independent of host nuclear machinery, enabling fast genome amplification and high burst sizes [16]. Unlike small DNA viruses, NDV compensates for genomic minimalism not through persistence, but through speed.

Broad Tropism and Low Host Specificity

In contrast to highly restrictive viruses such as HPV, NDV displays broad cellular tropism across avian and mammalian cells, largely determined by the ubiquitous distribution of sialic-acid-containing receptors recognised by the hemagglutinin–neuraminidase (HN) protein [17]. While NDV is highly pathogenic in birds, infection in humans is typically mild or asymptomatic, limited to transient conjunctivitis or flu-like symptoms [17].

This low host specificity allows NDV to replicate efficiently in a wide range of transformed and interferon-defective cells, a property directly linked to its small genome and limited immune-modulatory repertoire. NDV does not finely tune host responses; instead, it overwhelms them early.

Limited Intrinsic Immune Evasion but Strong Interferon Induction

NDV encodes only minimal innate immune antagonists (primarily the V protein), which are insufficient to fully suppress type I interferon responses in mammalian cells [18]. As a result, NDV infection is characterised by strong and rapid induction of interferon-stimulated genes. From a pathogenicity standpoint, this limits systemic spread. From a competitive standpoint, it confers a decisive advantage.

The intense early interferon burst induced by NDV can suppress the replication of co-infecting viruses, particularly those with slower replication cycles or that rely on immune evasion strategies [19]. Thus, NDV's small genome indirectly enables viral interference by prioritising replication speed over immune stealth.

NDV as a Competitive Virus in Coinfection

Within genome-size-driven viral competition models, NDV exemplifies the "speed-dominant" strategy. Its rapid transcription, high progeny output, and early immune activation allow NDV to dominate the early phase of coinfection, frequently restricting replication of larger or slower viruses [20,21].

Unlike large-genome viruses that encode multiple immune antagonists, NDV exerts competitive pressure through resource monopolisation and innate immune activation rather than molecular suppression. This makes NDV particularly effective at excluding viruses that require prolonged replication windows or immune quiescence.

High Utility in Modern Biotechnology

In sharp contrast to biologically passive small-genome viruses, NDV is extensively exploited in modern biotechnology and translational research:

- Oncolytic virotherapy: NDV selectively replicates in tumour cells with defective interferon signalling, inducing immunogenic cell death [22].
- Vaccine vector platforms: NDV is widely used as a live vector for heterologous antigen expression, despite its modest genome size, due to predictable transcription gradients and genetic stability [23].
- Immunostimulatory agent: NDV-induced interferon responses are harnessed to enhance antitumor and antiviral immunity [22].

Thus, NDV demonstrates that a small genome does not equate to biological irrelevance; rather, when paired with replication speed and immune activation, it becomes a powerful tool.

Evolutionary Dynamics of a Small RNA Genome

NDV's RNA-dependent RNA polymerase lacks proofreading activity, resulting in high mutation rates characteristic of RNA viruses [1]. This accelerates adaptation, host switching, and attenuation under selective pressure. However, the "rule of six" governing paramyxovirus genome length constrains excessive genomic expansion, preserving replication efficiency at the cost of functional diversity [16].

This evolutionary balance favours robustness and predictability—traits essential for NDV's long-standing use as both a vaccine strain and an oncolytic platform. Newcastle disease virus illustrates the productive extreme of small-genome viral design. Its limited genome enforces speed, early dominance, and strong immune activation, enabling both effective competition in coinfection and broad applicability in biotechnology. Unlike minimalist DNA viruses that persist quietly, NDV weaponises its simplicity—fast, loud, and useful.

1.7.3 Influenza A Virus: A Small Segmented Genome Built for Speed, Adaptation, and Platform Utility

Genome organisation and "compact versatility"

Influenza A virus (IAV) is an enveloped, negative-sense RNA virus with a segmented genome. Its

genetic economy is not "minimal" in the HPV sense; instead, IAV achieves functional breadth by distributing essential functions across segments and leveraging alternative splicing and accessory proteins. A practical consequence of segmentation is reassortment—rapid generation of novel genotype constellations when two influenza viruses co-infect the same cell—accelerating adaptation without requiring genome expansion.

For applied virology, the most important point is that IAV's genome is small enough to replicate efficiently yet structured enough to be engineered predictably using reverse genetics systems. Both studies explicitly rely on standard plasmid-based reverse genetics to generate recombinant influenza A viruses, underscoring the tractability of the IAV genome as an engineering substrate [24,25].

Replication strategy and competitive behaviour in coinfection

IAV replicates in a way that favours early dominance: rapid transcription/replication dynamics and high progeny output, followed by strong innate immune activation. In competitive terms, this combination often shifts the within-host environment toward interferon-stimulated restriction, narrowing the replication window for slower or more immune-sensitive viruses. While the two cited studies focus on vaccine vectors rather than coinfection ecology, they repeatedly emphasise the vector's immune-inductive targeting and induction of robust cellular responses—features consistent with influenza's ability to drive strong host responses [24,25].

NS1 as a control knob for attenuation and immunogenicity

A central engineering lever for IAV is the non-structural protein 1 (NS1). NS1 is widely used as an attenuation and antigen-delivery module because (i) it is abundantly expressed, (ii) it shapes host responses, and (iii) it can be genetically modified to reduce virulence while preserving immunogenicity. In the Veterinary World study, antigens were delivered via the NS1 region, and attenuation was achieved by modifying NS1 with a foreign sequence insertion [24]. In the MDPI *Vaccines* study, the influenza vector is characterised by truncation/mutation of NS1 and replacement of part of the coding region with heterologous antigen sequences, again highlighting NS1 as the "payload bay" for recombinant constructs [25]. Mechanistically, this strategy is supported by influenza NS1 biology literature cited within the provided papers (e.g., NS1's central role in infection biology) [24,25].

Influenza A as a biotechnology platform (vector vaccines)

Unlike viruses that are "too small to be useful," IAV is repeatedly demonstrated here as a practical vector platform:

- Native antigen expression and targeting of immune-inductive sites. The Veterinary World study notes influenza A vectors as advantageous for native antigen expression, targeting immunologically active sites, and scalable production [24].
- Predictable construction via reverse genetics. Both studies use established reverse genetics workflows to rescue recombinant viruses in cell culture and/or propagate them in embryonated eggs [24,25].
- Scalable manufacturing and stability options. The Veterinary World work emphasises rapid/scalable production using embryonated chicken eggs and reports candidate formulations, including an adjuvant-free approach with strong immunogenicity and simplified production [24].
- Demonstrated cellular immunogenicity in vivo. In calves, the Veterinary World study tracks IFNγ responses longitudinally and links post-vaccination IFNγ peaks to protective outcomes after challenge in their model system [24]. The *Vaccines* (MDPI) paper similarly uses protection indices (log CFU reductions) after challenge in mice and reports stronger protection in the adjuvant-free formulation [25].

Even though these are TB-antigen vector examples rather than influenza-antigen vaccines, they collectively illustrate the broader point: IAV's small segmented genome is not a limitation—it is a feature that enables stable, repeatable vectorisation.

Practical implications for "small-genome vs big-genome" framing

Within a genome-size/competition framing, IAV represents a "small-genome, high-impact" virus:

- It does not require large accessory gene sets to be competitive.
- It leverages replication efficiency, reassortment potential, and strong host-response modulation to shape outcomes.

- It is sufficiently genetically tractable to serve as a platform technology, especially when NS1 is used for attenuation and heterologous antigen delivery [24,25].

A decisive technological breakthrough in influenza research was the development of the eight-plasmid reverse genetics system by Hoffmann et al. [26]. This DNA transfection platform enables the rescue of fully infectious Influenza A virus entirely from cloned cDNA, allowing precise manipulation of each of the eight genomic RNA segments. The system provides unparalleled control over segment composition, attenuation markers, antigen insertion, and reassortment design. From a biotechnology standpoint, this method transformed Influenza A from a naturally adaptive virus into a programmable viral chassis. The recombinant vectors described in both cited vaccine studies rely on this reverse-genetics framework for the controlled generation and stability of engineered strains [24,25,26].

The non-structural protein 1 (NS1) occupies a central regulatory position in Influenza A biology. NS1 suppresses host antiviral signalling pathways, modulates interferon responses, influences host mRNA processing, and shapes viral pathogenicity [27]. Because NS1 is multifunctional yet genetically tolerant to truncations and insertions, it serves as a strategic locus for attenuation and heterologous antigen expression in vector-based vaccine design [24,25]. Rosário-Ferreira et al. [27] comprehensively describe NS1 as a molecular hub connecting viral replication efficiency with immune modulation. In recombinant influenza vectors, partial deletion or modification of NS1 reduces virulence while maintaining immunogenic capacity—an engineered balance between replication competence and safety. Thus, NS1 is not merely a virulence factor but a tunable regulatory switch. Influenza A aligns with broader principles of viral vector immunology. Draper and Heeney [28] outline the theoretical framework for viruses as vaccine vectors, emphasizing characteristics such as controlled attenuation, strong innate immune activation, scalable production, and capacity for heterologous antigen expression.

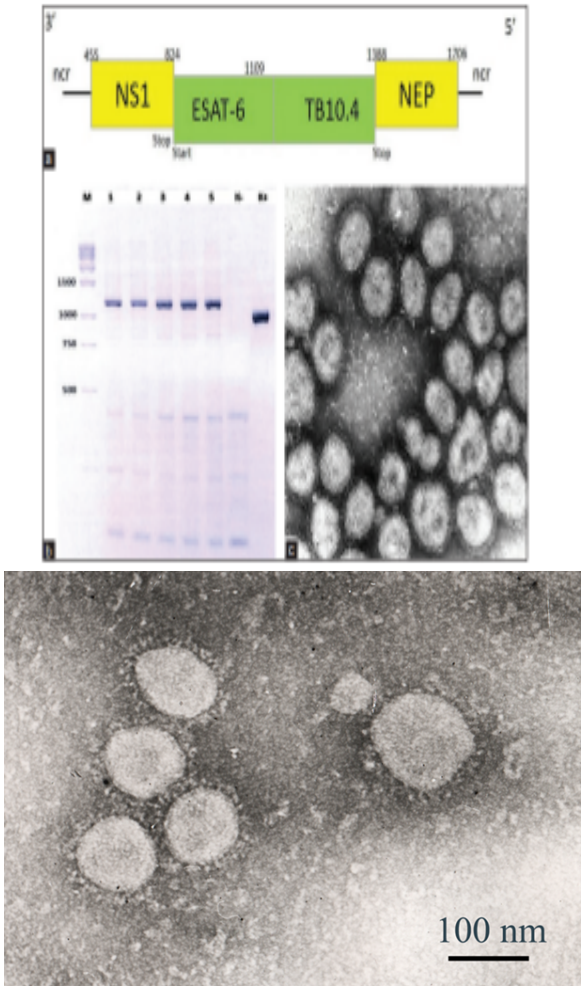

A B

Figure 3. Comparative transmission electron microscopy (TEM) of Influenza A virus and SARS-CoV-2 with reference to genome organisation and size. **(A) Influenza A virus (IAV).** Transmission electron microscopy image of recombinant Influenza A virions generated using plasmid-based reverse genetics, as described in the vector-based vaccine study [24]. Viral particles are pleomorphic to spherical, with diameters typically ranging from ~80–120 nm. Surface projections represent hemagglutinin (HA) and neuraminidase (NA) glycoproteins embedded in the host-derived lipid envelope. Influenza A contains a segmented negative-sense single-stranded RNA genome composed of eight segments with a total length of approximately 13.5 kb. The segmented genome organisation enables reassortment and facilitates genetic manipulation for vaccine vector development [24].

(B) SARS-CoV-2. Transmission electron microscopy of SARS-CoV-2 virions isolated from clinical material and propagated in Vero E6 cells, as reported in the MDPI *Viruses* study [29]. Viral particles appear spherical to mildly pleomorphic with diameters of ~80–120 nm (scale bar: 100 nm). Prominent spike (S) glycoproteins form the characteristic corona-like appearance. SARS-CoV-2 possesses a non-segmented positive-sense single-stranded RNA genome of approximately 29.9 kb—more than twice the size of Influenza A—encoding structural proteins (S, E, M, N) and multiple non-structural proteins including RNA-dependent RNA polymerase and proofreading exonuclease [29].

1. 7.4 Lethal Mutagenesis of SARS-CoV-2: Mechanistic Perspective Based on Tenofovir Prodrugs and Combination Antivirals

Lethal mutagenesis is an antiviral strategy that increases the viral mutation rate beyond the error threshold compatible with population survival, leading to error catastrophe and the collapse of the replicative pool. In RNA viruses, including SARS-CoV-2, this approach targets the RNA-dependent RNA polymerase (RdRp), promoting incorporation of mutagenic nucleoside analogues during genome replication.

Mechanistic Basis of SARS-CoV-2

SARS-CoV-2 possesses a ~29.9 kb positive-sense RNA genome and encodes an RdRp complex (nsp12-nsp7-nsp8) with associated proofreading exonuclease (nsp14-ExoN). This proofreading activity partially limits the effectiveness of mutagenic nucleoside analogues by excising misincorporated nucleotides. Therefore, successful lethal mutagenesis in coronaviruses requires either:

1. High analogue incorporation rates that overwhelm ExoN correction; or
2. Combination strategies that impair proofreading or synergistically increase mutational burden.

The morphological integrity of SARS-CoV-2 virions (B.1 lineage) propagated in Vero E6 cells. Transmission electron microscopy (TEM) (see Figures 10–11, pp. 20–22) confirms that the antiviral effects observed in vitro are not due to structural artefacts but occur at the replication level [29].

Tenofovir Prodrugs and Theoretical Mutagenesis Potential

Tenofovir disoproxil fumarate (TDF) and tenofovir alafenamide (TAF) are nucleotide reverse transcriptase inhibitors (NtRTIs) primarily designed for HIV therapy. Their active metabolite, tenofovir diphosphate (TFV-DP), acts as a chain terminator in retroviral DNA synthesis. However, when evaluated against SARS-CoV-2 in vitro, both compounds demonstrated significant viral load reduction under defined MOI conditions (MOI 2 for TDF; MOI 0.01 for TAF), with time-dependent enhancement of antiviral effect.

In the MDPI *Viruses* study (2025) [29], lethal mutagenesis was inferred from:

- Reduction in $TCID_{50}$ viral titers,
- Dose-dependent inhibition curves (Figures 4–6),
- Time-dependent antiviral enhancement up to 96 h exposure (Figures 8–9),
- Conceptual model of RdRp error induction (Figure 5, p. 13)

Although direct whole-genome sequencing confirmation of the mutation spectrum was not performed, the data suggest that, at sufficiently high intracellular concentrations, tenofovir metabolites may contribute to increased replication errors or incomplete RNA elongation.

Importantly, the presence of the ExoN proofreading complex remains a mechanistic barrier. Therefore, tenofovir alone is unlikely to induce classical error catastrophe at physiological concentrations, but may contribute to mutational pressure when used in combination regimens.

Synergistic Mutagenesis: Favipiravir and Ribavirin

The synergistic inhibition study by Khaidarov et al. (2026) [30] demonstrated quantitative Combination Index (CI) values <1 for the favipiravir-ribavirin combination, confirming pharmacodynamic synergy in SARS-CoV-2 inhibition. Favipiravir, a known RNA mutagen, and ribavirin, which induces transition mutations and depletes GTP pools, collectively increase the mutational burden of viral RNA synthesis [30].

In contrast to tenofovir, favipiravir directly targets RdRp fidelity, promoting accumulation of deleterious substitutions. Quantitative CI/DRI modelling indicated:

- Enhanced $\log_{10}$ viral load reductions beyond additive expectations,
- Dose reduction indices supporting therapeutic window optimisation,

- Synergistic antiviral pressure at clinically achievable concentrations.

Thus, while tenofovir's mutagenic contribution may be mechanistically limited by proofreading, favipiravir-based regimens demonstrate a more classical lethal mutagenesis profile.

The following summary can be made:

1. SARS-CoV-2 virion integrity is maintained post-treatment, indicating replication-targeted rather than structural disruption [29]
2. Tenofovir prodrugs exhibit dose- and time-dependent suppression, potentially involving partial chain termination and limited mutagenic effects.
3. Favipiravir–ribavirin combinations show quantitative synergy consistent with lethal mutagenesis mechanisms [30].
4. Proofreading exonuclease activity remains a critical determinant of mutagenesis efficacy.

Therefore, lethal mutagenesis in SARS-CoV-2 likely requires:

- Potent RdRp error inducers,
- Combination strategies to exceed proofreading capacity,
- Sustained intracellular exposure to reach the mutational tipping point.

1.7.5. SARS-CoV-2 Genome Architecture and the nsp14 Exoribonuclease: Implications for Replication Fidelity and Lethal Mutagenesis

SARS-CoV-2 possesses one of the largest known RNA virus genomes (~29.9 kb), a defining feature of coronaviruses within the order *Nidovirales*. Genome expansion in coronaviruses has been mechanistically linked to the acquisition of a 3′→5′ exoribonuclease (ExoN) activity encoded by the nonstructural protein 14 (nsp14), which enhances replication fidelity and permits the maintenance of a large coding capacity [31-34].

Genomic Organization and Replicase Complexity

The SARS-CoV-2 genome comprises:

- ORF1a/ORF1ab encoding the replicase polyproteins (nsps 1–16),
- Structural proteins (S, E, M, N),
- Multiple accessory proteins.

Within ORF1ab, nsp14 is bifunctional, containing:

1. An N-terminal 3′→5′ ExoN domain with conserved DEDDh catalytic motifs,
2. A C-terminal guanine-N7-methyltransferase (N7-MTase) domain.

Sequence alignment across betacoronaviruses demonstrates strong conservation of ExoN catalytic residues and zinc finger motifs, underscoring its evolutionary stability [33]. The structural organisation of nsp14 enables proofreading during RNA synthesis and contributes to the unusually high fidelity of coronavirus replication compared to that of other RNA viruses [31,33].

ExoN as a Determinant of Genome Size and Fidelity

Typical RNA viruses replicate near an error threshold beyond which accumulated mutations lead to population collapse. Coronaviruses differ by encoding ExoN-mediated proofreading, thereby reducing mutation rates and allowing expansion to ~30 kb genomes [31,33].

Biochemical and reverse-genetics data demonstrate that catalytic inactivation of ExoN residues in SARS-CoV-2 prevents recovery of infectious virus [33]. Unlike some related coronaviruses, where ExoN inactivation results in a viable mutator phenotype, SARS-CoV-2 ExoN mutants are replication-defective, indicating that proofreading is tightly coupled to RNA synthesis. Importantly, ExoN inactivation does not disrupt nsp14's N7-MTase function, confirming functional domain independence [33].

These findings imply that ExoN is not merely an accessory fidelity factor but an essential replication determinant in SARS-CoV-2.

nsp14–nsp10 Interface and Replication Complex Stability

ExoN activity is strongly stimulated by interaction with nsp10. Structural and biochemical analyses reveal that the nsp14–nsp10 interface stabilises the catalytic site and enhances RNA-binding and exonucleolytic efficiency [31,33]. Disruption of this interface significantly reduces RNA synthesis efficiency and compromises replication complex assembly [31].

Thus, the proofreading system operates as a multi-protein module integrated within the RdRp complex (nsp12–nsp7–nsp8–nsp10–nsp14). This structural dependency reinforces ExoN's central role in maintaining genome integrity.

Genome Size, RNA Interactions, and Host Modulation

The large SARS-CoV-2 genome generates abundant genomic and subgenomic RNAs during infection. Viral RNAs in other RNA virus systems have been shown to sequester cellular RNA-binding proteins and modulate host responses through RNA "sponging" mechanisms [32]. Although this phenomenon has been extensively documented in other RNA viruses, the principle that abundant viral RNAs can reshape host RNA-protein networks is relevant to understanding coronavirus-host interactions [32].

Given the high intracellular levels of SARS-CoV-2 RNAs, similar RNA-mediated modulation of host RNA-binding proteins may contribute to replication efficiency and cytopathology, although this requires direct experimental validation.

Implications for Lethal Mutagenesis

Lethal mutagenesis strategies aim to elevate mutation rates beyond the tolerable threshold. However, SARS-CoV-2 proofreading via nsp14 imposes a significant barrier to mutagenesis-based antiviral approaches:

- ExoN excises misincorporated nucleotides,
- Catalytic inactivation is nonviable,
- Proofreading is functionally coupled to primary RNA synthesis [33].

Therefore, successful lethal mutagenesis in SARS-CoV-2 must either:

1. Overwhelm ExoN's proofreading capacity, or
2. Functionally disrupt the nsp14–nsp10 interface without completely abolishing replication.

The structural and enzymatic data collectively demonstrate that SARS-CoV-2 genome size, replication fidelity, and proofreading capacity are mechanistically interconnected [32,33]. Any mutagenesis-based strategy must account for this integrated replication-fidelity system.

1.7.6 Kazakhstan's strain of SARS-CoV2 NSP12 and 14

Full-genome sequencing of SARS-CoV-2 isolates circulating in Kazakhstan revealed characteristic mutations in the replication complex, particularly within NSP12 (RNA-dependent RNA polymerase, RdRp) and NSP14 (Exoribonuclease/ExoN), both central to viral replication fidelity and evolutionary dynamics.

The complete genome of the strain SARS-CoV-2/human/KAZ/B1.1/2021 was determined to be 29,815 nt, while SARS-CoV-2/human/KAZ/Britain/2021 comprised 29,751 nt, covering all coding regions including ORF1ab, structural, and accessory genes. Sequencing and phylogenetic analysis assigned the strains to lineages B.1.1 and B.1.1.7, respectively, consistent with global circulating variants during the pandemic period [31].

Mutations in NSP12 (RdRp)

NSP12 forms the catalytic core of the replication–transcription complex. Comparative analysis with the Wuhan reference strain (NC_045512.2) identified the well-characterised C14408T mutation resulting in P314L substitution, detected in both Kazakh isolates. This mutation has been widely associated with increased viral fitness and co-occurs with spike D614G globally. Additional synonymous and non-synonymous substitutions were identified in NSP12 (e.g., A517V, P218L), reflecting lineage-specific diversification.

The structural and functional importance of NSP12 in RNA synthesis and as a target of nucleoside analogues (e.g., remdesivir, favipiravir) underscores the need to monitor its genetic variability [31].

Mutations in NSP14 (ExoN)

NSP14 is a bifunctional protein containing:

- An N-terminal 3′–5′ exoribonuclease (ExoN) responsible for proofreading.
- A C-terminal N7-methyltransferase domain involved in RNA capping.

The proofreading activity of NSP14, enhanced by its interaction with NSP10, distinguishes coronaviruses from most RNA viruses by significantly increasing replication fidelity. Mutational analysis revealed substitutions in NSP14 in the Kazakh strains, including lineage-associated changes within ORF1ab regions corresponding to ExoN domains [31].

Given that ExoN activity counteracts lethal mutagenesis by excising misincorporated nucleotides, genomic surveillance of NSP14 is critical when evaluating nucleoside analogue–based antiviral strategies.

Genome Organisation Context

SARS-CoV-2 possesses a large positive-sense RNA genome (~29.9 kb), among the largest known for RNA viruses. ORF1ab encodes 16 non-structural proteins (NSP1–NSP16) that form the replication–transcription complex. Structural genes (S, E, M, N) and accessory ORFs follow in the 3′ region.

The Kazakh isolates preserved canonical genome architecture while demonstrating expected lineage-defining mutations in Spike, Nucleocapsid, and replication-associated proteins. The overall mutational landscape confirmed ongoing adaptation without disruption of essential replication domains

1.7.7 Lethal Mutagenesis in HIV-1

Human immunodeficiency virus type 1 (HIV-1) is a retrovirus with a ~9.7 kb single-stranded, positive-sense RNA genome that is reverse-transcribed into DNA by a virally encoded reverse transcriptase (RT). A defining biological feature of HIV-1 replication is the absence of proofreading activity in RT, resulting in high mutation rates and continuous generation of genetically diverse quasispecies populations [1,2]. This intrinsic genetic variability underlies both rapid adaptability and vulnerability to error catastrophe.

Mutation Rate, Quasispecies, and Error Threshold

RNA viruses—including retroviruses—replicate near a critical error threshold, balancing genetic diversity with maintenance of functional genomes [1,3]. According to quasispecies theory, excessive accumulation of deleterious mutations leads to progressive fitness loss and ultimately population collapse, a process often described as Muller's ratchet [2,3].

Experimental studies have demonstrated that increasing mutation frequency through mutagenic nucleoside analogues can push viral populations beyond this tolerable threshold. In HIV-1, treatment with mutagenic nucleosides has been shown to induce lethal mutagenesis, characterised by elevated G→A and transition mutations, reduced infectivity, and progressive extinction of viral replication capacity [4].

Mechanism of Lethal Mutagenesis in HIV-1

Lethal mutagenesis exploits the lack of RT proofreading by introducing nucleoside analogues that are incorporated into nascent viral DNA during reverse transcription [32-35]. The process involves:

1. Mutagen incorporation during reverse transcription;
2. Increased mispairing frequency during DNA synthesis;
3. Accumulation of deleterious mutations across viral genomes;
4. Fitness decline and replication failure once the mutation threshold is exceeded.

Unlike coronaviruses, HIV-1 lacks a dedicated exonuclease proofreading system, making it particularly susceptible to mutagen-driven error accumulation [32,35].

Ribavirin and Mutagenic Nucleosides in HIV Context

Ribavirin and other mutagenic nucleoside analogues have been shown to increase mutation frequency in multiple RNA viruses, including HIV-1 [33,36]. Loeb et al. demonstrated that mutagenic nucleosides can induce lethal mutagenesis in HIV by elevating the mutation burden to nonviable levels [35]. These findings established the principle that, due to their inherently high mutation rates, retroviruses can be therapeutically pushed beyond their error threshold.

However, the effectiveness of lethal mutagenesis depends on maintaining a delicate balance: sufficient mutational pressure must be applied to drive viral extinction while avoiding unacceptable toxicity to host cells [32,35].

Therapeutic Considerations

Although lethal mutagenesis imposes a high genetic barrier to resistance, several constraints must be considered:

- Host toxicity: Mutagenic nucleosides may affect host polymerases or mitochondrial DNA replication [32,35].
- Selective pressure: Sublethal mutagenesis may promote adaptive variants rather than extinction if mutational burden remains below threshold [33,34].
- Therapeutic window: Effective viral extinction requires sustained mutational pressure within tolerable dosing limits [32].

In HIV-1, the absence of proofreading provides a mechanistic advantage for mutagenesis-based therapy compared to large-genome RNA viruses. However, the high adaptability of HIV-1 necessitates precise dosing strategies to ensure collapse rather than selection.

In the HIV-1 context, lethal mutagenesis is theoretically well supported by quasispecies dynamics and experimental validation. The virus replicates near its error threshold due to error-prone reverse transcription. Pharmacological elevation of mutation rates can induce catastrophic fitness decline and viral extinction. Therefore, HIV-1 remains one of the most conceptually suitable targets for mutagenesis-driven antiviral strategies.

Schematic representation (Figure 4) of the lethal mutagenesis process in human immunodeficiency virus type 1 (HIV-1). Following

infection of a $CD4^+$ target cell, the viral single-stranded RNA genome (~9.7 kb) undergoes reverse transcription by the viral reverse transcriptase (RT), an enzyme lacking proofreading exonuclease activity. In the presence of a mutagenic nucleotide analogue, erroneous nucleotides are incorporated into nascent proviral DNA during RT-mediated synthesis. This results in increased mutation frequency within the integrated proviral genome. Progressive accumulation of deleterious mutations across replication cycles elevates the mutational burden beyond the viral error threshold, leading to loss of infectivity, reduced replication competence, and eventual collapse of the viral population (error catastrophe).

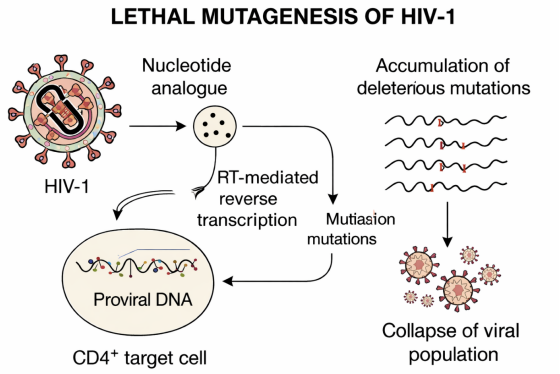

Figure 4. Mechanistic model of lethal mutagenesis in HIV-1 mediated by nucleotide analogue incorporation during reverse transcription.

HIV-1 replication is characterised by exceptionally high genetic turnover driven by the intrinsic infidelity of reverse transcriptase, which lacks proofreading exonuclease activity. Viral production rates of approximately 10^7–10^9 virions per day, combined with an estimated mutation rate of ~3 × 10^{-5} mutations per base per replication cycle, result in the continuous generation of genetically diverse quasispecies populations [39]. Consequently, virtually every possible single-nucleotide substitution—and many double mutations—may arise daily within an infected individual [39]. This extensive mutational plasticity underlies rapid viral adaptation and the emergence of drug resistance through selection of preexisting minority variants under antiretroviral pressure [39].

The evolutionary dynamics of HIV-1 reflect a balance between mutation-driven diversity and preservation of replication competence. Although resistance mutations provide selective advantage in the presence of antiretroviral agents, many impose replication fitness costs in drug-free environments until compensatory mutations restore viral capacity [39]. These clinical and molecular observations indicate that HIV-1 populations operate near a functional error threshold, where excessive accumulation of deleterious mutations can compromise viral viability.

This conceptual framework directly relates to the theory of error catastrophe. If mutation frequency exceeds the tolerable threshold, progressive accumulation of deleterious substitutions results in loss of infectivity and eventual population collapse. While conventional antiretroviral therapy selects for fitter resistant variants, the same high baseline mutation rate that facilitates resistance also renders HIV-1 theoretically susceptible to mutagenesis-based antiviral strategies designed to increase mutational load beyond sustainable limits [39]. Thus, HIV-1 provides a clinically validated model linking mutational burden, viral fitness, and evolutionary selection.

The MT-4 human T-lymphoblastic cell line represents one of the most extensively characterized in vitro systems for studying HIV-1 replication and antiviral intervention. Owing to its high permissivity to HIV-1 infection, MT-4 cells rapidly develop pronounced cytopathic effects (CPE), including syncytium formation and progressive cell death. This robust and reproducible cytopathogenic response has established MT-4 cells as a standard model for mechanistic studies of viral replication and for the evaluation of antiviral compounds.

HIV-1 entry into MT-4 cells is initiated by interaction of the viral envelope glycoprotein gp120 with the CD4 receptor and the CXCR4 co-receptor, followed by membrane fusion mediated by gp41. Subsequent reverse transcription of the viral RNA genome, integration of proviral DNA into the host genome, and productive replication culminate in extensive loss of cell viability. This virus-induced cytotoxicity provides a quantitative readout for assessing viral replication dynamics in vitro.

Among cell-based anti-HIV assays, the **MTT viability** assay remains a widely applied method for indirectly measuring viral cytopathogenicity and compound-mediated protection. The assay is based on the reduction of the tetrazolium salt 3-(4,5-

dimethylthiazol-2-yl)-2,5-diphenyltetrazolium bromide (MTT) by metabolically active cells into insoluble formazan crystals, which are subsequently solubilised and quantified spectrophotometrically at 570 nm. In the context of HIV-1 infection, decreased absorbance reflects virus-driven metabolic impairment and cell death, whereas restoration of signal in treated cultures indicates preservation of cell viability and antiviral activity.

Quantitative analysis of MTT-derived absorbance values allows calculation of percentage protection relative to virus and cell controls and determination of half-maximal effective concentrations (EC_{50}). Thus, the MT-4/MTT system integrates virological, cytopathological, and pharmacodynamic parameters into a single functional platform.

Importantly, HIV-1 reverse transcriptase lacks proofreading exonuclease activity, rendering viral replication intrinsically error-prone and generating highly diverse quasispecies populations. This high mutation rate both facilitates rapid adaptation and creates vulnerability to error amplification. Consequently, the MT-4/MTT model is not only suitable for evaluating classical inhibitors of viral entry, integration, or replication, but also provides a relevant framework for investigating mutagenesis-based antiviral strategies targeting reverse transcription and quasispecies stability.

Fluorescence-based reporter systems have become valuable tools for monitoring HIV-1 replication in cell culture. In EGFP-reporter models, viral replication activates Tat-dependent transcription from the HIV-1 long terminal repeat (LTR), resulting in enhanced green fluorescent protein (EGFP) expression. Compounds with antiviral activity interfere with steps of the HIV-1 replication cycle, leading to reduced Tat-mediated transcriptional activation and, consequently, decreased EGFP fluorescence. Quantification of EGFP expression can be achieved using automated fluorescence microscopy or flow cytometry, enabling sensitive and reproducible assessment of antiviral activity.

Compared with conventional cytopathic effect (CPE)-based assays, EGFP-reporter assays offer several methodological advantages. First, EGFP is intrinsically fluorescent and does not require the addition of exogenous substrates, allowing a homogeneous, non-destructive, and mix-and-read workflow. Because the detection method does not compromise cell viability, plates can be analyzed repeatedly over time, providing experimental flexibility while reducing reagent costs. Second, fluorescence is detectable prior to overt virus-induced cytotoxicity, enabling measurement of viral replication in viable cells and shortening the overall incubation period, as the assay does not depend on end-stage life–death discrimination. Third, fluorescence microscopy permits archiving of images and raw quantitative data, facilitating subsequent analysis and validation.

A potential limitation of fluorescence-based reporter systems is interference from intrinsically fluorescent compounds or serum components, which may confound signal interpretation. Therefore, appropriate controls and secondary validation assays remain essential when screening compound libraries.

1.7.8. Combination Pressure and Genome-Dependent Sensitivity: Lessons from HIV Synergy Models

Combination antiviral strategies provide a mechanistic framework for understanding how genome architecture influences susceptibility to competitive or mutational stress. In vitro synergy studies involving the NNRTI ACC007 combined with lamivudine (3TC) and tenofovir disoproxil fumarate (TDF) demonstrated significant cooperative inhibition of HIV-1 replication, with combination indices (CIs) < 1 and substantial dose-reduction indices across viral strains [39].

Although HIV-1 differs from RNA respiratory viruses in replication strategy, the principle is instructive: multi-target pressure reduces the effective concentration required for viral suppression, indicating that replication systems can be destabilized by convergent inhibitory mechanisms.

In the context of nucleotide analogues relevant to RNA viruses, concentration normalisation is critical when comparing antiviral thresholds across genome classes.

Using the conversion:

$$\mu g/mL = nM \times MW\ (g/mol) \times 10^{-6}$$

and standard molecular weights:

- Tenofovir disoproxil fumarate (TDF): 635.5 g/mol
- Tenofovir alafenamide (TAF): 476.47 g/mol

The corresponding converted concentrations are:

- TDF, 14 nM
  $14 \times 635.5 \times 10^{-6} = 0.0089$ µg/mL
- TAF, 5 nM
  $5 \times 476.47 \times 10^{-6} = 0.0024$ µg/mL

These values illustrate that sub-10 nM concentrations correspond to low microgram-per-milliliter ranges, emphasizing that modest molar exposures can exert measurable antiviral pressure when synergy is present.

Relevance to Genome Size–Dependent Competitive Dynamics

The HIV combination model demonstrates a broader biological principle:

1. Single-agent pressure may be insufficient for viruses with robust replication buffering mechanisms.
2. Synergistic combinations lower the collapse threshold of viral replication systems.
3. Multi-axis targeting can destabilize replication complexes more effectively than monotherapy.

When translated to the small- vs large-genome virus framework:

- Small-genome RNA viruses (e.g., Influenza A virus) lack proofreading and are highly susceptible to single mutagenic agents such as favipiravir.
- Large-genome RNA viruses, particularly SARS-CoV-2, encode proofreading machinery (nsp14-ExoN), which increases tolerance to mutational pressure.
- As a result, combination pressure may be required to approach functional lethal mutagenesis thresholds in large-genome viruses.

Thus, antiviral synergy data serve as an experimental analogue of viral competition under constrained intracellular resources: destabilisation of replication-fidelity mechanisms shifts the balance between rapid, small-genome replicators and fidelity-optimised, large-genome viruses.

2. Materials

Antivirals

Tenofovir alafenamide (TAF) ≥98% (HPLC), HIV and HBV reverse transcriptase inhibitor, powder (Merck, Sigma-Aldrich, KGaA, Darmstadt, Germany)

Tenofovir Disoproxil Fumarate (TDF) Viread ≥99% HIV and HBV reverse transcriptase inhibitor, tablets, (333 Lakeside Drive, Foster City, CA 94404, USA)

2.1. Cells and Virus

HIV-1 strain. The HIV-1 (CRF07_BC) laboratory strain was kindly provided by Beijing Institute of Microbiology and Epidemiology. Viral stocks were propagated and titrated according to standard procedures in MT4 cells. MT4 cells (human T-lymphotropic virus type 1-transformed human T lymphoblastoid cell line) was purchased at Sunncell, LLP, Wuhan, China - product SNL-377 with a valid STR profile These cells were generated by stable transfection of MT4 cells with a construct containing the HIV-1 long terminal repeat (LTR) promoter driving enhanced green fluorescent protein (EGFP) expression, followed by antibiotic selection of stable clones as described. The cells were obtained by stable transformation of MT4 cells with a CMV promoter-driven EGFP construct [37].

MTT-assay

The MT-4 human T-lymphoblastic cell line (HTLV-1–transformed) was used as a highly permissive host for HIV-1 infection. *Cells* were cultured in RPMI-1640 supplemented with 10% fetal bovine serum (FBS), penicillin, and streptomycin, and maintained at 37 °C in a humidified atmosphere containing 5% CO_2. HIV-1 stocks were propagated in MT-4 cells and titrated prior to use in experiments. Viral multiplicity of infection (MOI) was selected to induce substantial cytopathic effect (CPE) within 4–5 days post-infection

2.2 Reagents and Consumables

The reagents and solvents were obtained commercially. RPMI-1640 medium supplemented with Ultra Glutamine and HEPES (without phenol red) was obtained from Lonza-Bio Whittaker® (Lonza, Basel, Switzerland). The medium was supplemented with 10% fetal bovine serum (FBS; Sigma-Aldrich, St. Louis, MO, USA) and 0.02 mg/mL gentamicin (Gibco, Thermo Fisher Scientific, Waltham, MA, USA). Geneticin® (G418; Gibco, Thermo Fisher Scientific) was used for the selection and maintenance of stably transfected MT4-derived cell lines.

Corning® 384-well flat clear-bottom black polystyrene TC-treated microplates and Corning® 96-well clear V-bottom TC-treated microplates were purchased from Corning Inc. (Corning, NY, USA). Standard tissue culture flasks (T-25, T-75) were used for routine cell maintenance under sterile conditions.

MTT-assay

MT-4 cells were cultured in RPMI-1640 medium (Gibco, Thermo Fisher Scientific, Waltham, MA, USA) supplemented with 10% fetal bovine serum (FBS; Sigma-Aldrich, St. Louis, MO, USA), 100 U/mL penicillin, and 100 µg/mL streptomycin (Gibco).

HIV-1 viral stocks were prepared and titrated in MT-4 cells.

Test compounds were dissolved in dimethyl sulfoxide (DMSO; Sigma-Aldrich) and diluted in complete medium to the desired concentrations.

MTT (3-(4,5-dimethylthiazol-2-yl)-2,5-diphenyltetrazolium bromide) was obtained from Sigma-Aldrich and prepared as a 5 mg/mL stock solution in phosphate-buffered saline (PBS; Gibco). Formazan crystals were solubilised using 10% sodium dodecyl sulfate (SDS; Sigma-Aldrich) in 0.01 M HCl or acidified isopropanol.

HIV-1 p24 antigen levels were quantified using a commercial p24 antigen capture ELISA kit (e.g., Cell Biolabs, Inc., San Diego, CA, USA) according to the manufacturer's instructions. Where required, viral supernatants were treated with Triton X-100 (Sigma-Aldrich) prior to analysis.

MTT assays were performed in 96-well flat-bottom tissue culture plates (Corning Inc., Corning, NY, USA). Syncytium formation assays were conducted in 24- or 48-well tissue culture plates (Corning).

2.3 Equipment

Cell counting was performed using a Z2™ Coulter Counter® Analyzer (Beckman Coulter, Brea, CA, USA). Cells were incubated in a humidified incubator at 37 °C with 5% CO_2. Centrifugation steps were carried out using an Allegra® X-15R centrifuge (Beckman Coulter). Compound dispensing for high-throughput screening (HTS) assays was performed using a Multidrop™ Combi reagent dispenser (Thermo Fisher Scientific). Fluorescence measurements were conducted using an automated fluorescence microscope equipped with a 488 nm excitation laser or, alternatively, a fluorescence spectrophotometer suitable for EGFP detection.

MTT-assay

Absorbance measurements were obtained using a microplate reader (BioTek Instruments, Winooski, VT, USA) at 570 nm (MTT assay)

3. Methods

3.1 Preparation of Virus Stocks

Cell numbers were determined using a Z2™ Coulter Counter® Analyser (Beckman Coulter, Brea, CA, USA). Cells were cultured at 37 °C in a humidified atmosphere containing 5% CO_2.

Centrifugation steps were performed using an Allegra® X-15R centrifuge (Beckman Coulter, Brea, CA, USA). Compounds were dispensed for high-throughput screening (HTS) assays using a Multidrop™ Combi reagent dispenser (Thermo Fisher Scientific, Waltham, MA, USA). Fluorescence measurements were acquired using an automated fluorescence microscope equipped with 488 nm excitation or a fluorescence spectrophotometer configured for EGFP detection (488 nm excitation, 510–520 nm emission).

MTT-assay

HIV-1 virus stocks were generated by infecting exponentially growing MT-4 cells maintained in complete RPMI-1640 medium supplemented with 10% fetal bovine serum. Cells were cultured at 37 °C in a humidified atmosphere containing 5% CO_2 and monitored daily for the development of cytopathic effects, including syncytium formation and progressive cell death. Upon extensive cytopathic effects, culture supernatants were collected, clarified by low-speed centrifugation to remove cellular debris, and aliquoted to avoid repeated freeze–thaw cycles. Viral stocks were stored at −80 °C until use.

Virus titers were determined in MT-4 cells prior to experimental application to ensure reproducible infection conditions in the MTT-based antiviral assay. The multiplicity of infection was selected to induce a significant cytopathic effect within 4–5 days, consistent with the dynamic range required for reliable assessment of compound-mediated protection

3.2 Titration of the Virus Stocks

Virus dilutions were prepared in 96-well V-bottom plates using the following layout: column 1 served as the medium control (MC), columns 2–11 as a fivefold serial dilution of the virus, and column 12 as the cell control (CC). To determine viral titers ($TCID_{50}$/mL), a dilution series was performed in octuplicate (rows A–H).

RPMI/10% FBS (100 µL) was dispensed into column 1 (MC) and columns 3–12 using a multichannel pipette or Multidrop™ Combi reagent dispenser (Thermo Fisher Scientific, Waltham, MA, USA). Virus stocks were thawed at 37 °C, and 125 µL of undiluted virus was added to each well of column 2.

Fivefold serial dilutions were prepared by transferring 25 µL from column 2 into 100 µL RPMI/10% FBS in column 3, mixing thoroughly, and subsequently transferring 25 µL to the next column. This process was repeated through column 11. RPMI/10% FBS containing 2% DMSO was prepared (4 mL per 384-well plate). Ten microliters of this solution were dispensed into each well of a 384-well black plate using a Multidrop™ Combi reagent dispenser. For quadruplicate testing, 15 µL from each well of the 96-well plate was transferred into corresponding quadruplicate wells of the 384-well plate (e.g., well A1 of the 96-well plate was transferred to wells A1, A2, B1, and B2 of the 384-well plate). MT4-LTR-EGFP cells were prepared at 4 × 10^5 cells/mL in RPMI/10% FBS (6 mL per 384-well plate). Fifteen microliters of the cell suspension were dispensed into columns 3–24 of the 384-well plate using a Multidrop™ Combi reagent dispenser. Columns 3–22 contained serial virus dilutions, while columns 23 and 24 served as cell controls (CC). Fifteen microliters of RPMI/10% FBS was dispensed into columns 1 and 2 as medium controls (MC). Plates were incubated for 3 days at 37 °C in a humidified atmosphere containing 5% CO_2. After incubation, wells exhibiting cytopathic effect (CPE) or fluorescence were scored for each virus dilution. Viral titers ($TCID_{50}$/mL) were calculated using the Reed–Muench method [38].

MTT-Assay

Virus titers were determined in MT-4 cells to ensure standardised infection conditions for subsequent antiviral assays. Briefly, serial dilutions of clarified HIV-1 stock were prepared in complete RPMI-1640 medium and added to MT-4 cells seeded in 96-well plates. Cells were incubated at 37 °C in a humidified atmosphere containing 5% CO_2 and monitored for the development of cytopathic effects over 4–5 days.

Viral replication was evaluated by the extent of cytopathic effect and by reduction in cell viability, as measured by the MTT assay. The tissue culture infectious dose required to infect 50% of cell cultures ($TCID_{50}$/mL) was calculated using the Reed–Muench method. The calculated viral titer was subsequently used to define the multiplicity of infection applied in antiviral activity assays, ensuring consistent and reproducible induction of cytopathic effects within the defined incubation period

3.3. HIV-1 Antiviral High-Throughput Screening Assay

3.3.1 Preparation of the Compound Test Plates

Fourfold serial dilutions of test compounds were prepared in RPMI/10% FBS at four times the final assay concentration. Stock solutions were prepared in 100% DMSO and subsequently diluted in culture medium to the desired concentrations. Ten microliters of each dilution were dispensed into columns 3–22 of 384-well black plates, resulting in a final DMSO concentration of 2% per well. Typically, four concentrations per compound were tested, with up to 80 compounds evaluated per plate. For each compound set, duplicate plates were prepared: one for antiviral activity assessment and one for cytotoxicity evaluation. For antiviral activity plates, 10 µL of RPMI/10% FBS containing 2% DMSO was dispensed into columns 1, 2, 23, and 24. In this layout, columns 1 and 2 served as virus control (VC; virus without compounds), columns 3–22 contained serial dilutions of test compounds, and columns 23 and 24 served as cell control (CC; cells without virus and compounds). For cytotoxicity plates, 10 µL of RPMI/10% FBS containing 2% DMSO was dispensed into columns 1, 2, 23, and 24. In this format, columns 1 and 2 served as cell control (CC; cells without compounds), columns 3–22 contained serial dilutions of test compounds, and columns 23 and 24 served as medium control (MC; medium without cells and compounds).

MTT-assay

For high-throughput antiviral screening, test compounds were prepared as stock solutions in dimethyl sulfoxide (DMSO) and diluted in complete RPMI-1640 medium to obtain fourfold serial dilutions at four times the intended final assay concentration. Aliquots (10 µL per well) were dispensed into 384-well black tissue culture plates. The final DMSO concentration in each well was kept constant and did not exceed cytotoxic levels.

For antiviral activity assessment, columns designated as virus control contained infected cells without compound, while cell control wells contained uninfected cells. Wells assigned for compound testing contained serial dilutions of each compound. Duplicate plates were prepared in parallel to evaluate cytotoxicity in the absence of virus infection.

This plate configuration enabled simultaneous determination of antiviral activity and cytotoxicity

under identical experimental conditions, ensuring accurate calculation of EC_{50}, CC_{50}, and selectivity index values within the MT-4–based fluorescence or viability readout system

3.3.2 Antiviral Testing

HIV-1 Infection and Cytotoxicity Assay Procedure

For antiviral activity testing, MT4-LTR-EGFP cells were prepared at 4×10^5 cells/mL in RPMI/10% FBS (6 mL per 384-well plate). For cytotoxicity evaluation, MT4-CMV-EGFP cells were prepared at 2×10^5 cells/mL in RPMI/10% FBS (12 mL per 384-well plate). Virus stocks were thawed at 37 °C and diluted in RPMI/10% FBS to obtain a multiplicity of infection (MOI) of 0.0025 $TCID_{50}$/cell. A total of 6 mL of virus dilution was prepared per 384-well activity plate. For example, when using a virus stock with a titer of 3.33×10^5 $TCID_{50}$/mL, 3 µL of virus stock per mL of dilution was required to achieve the desired MOI. For antiviral activity plates, 15 µL of RPMI/10% FBS was dispensed into columns 23 and 24. Fifteen microliters of virus dilution was dispensed into columns 1–22. Subsequently, 15 µL of MT4-LTR-EGFP cell suspension (6,000 cells/well) was added to all wells.

For cytotoxicity plates, 30 µL of RPMI/10% FBS was dispensed into columns 23 and 24. Thirty microliters of MT4-CMV-EGFP cell suspension (6,000 cells/well) was dispensed into columns 1–22. Plates were incubated for 3 days at 37 °C in a humidified atmosphere containing 5% CO_2. At 3 days post-infection, EGFP fluorescence was quantified using an automated fluorescence microscope with 488 nm excitation. *MTT-assay*

Antiviral activity and cytotoxicity were evaluated using the MTT assay in MT-4 cells as previously described. Briefly, MT-4 cells were seeded in microtiter plates at a density sufficient to maintain exponential growth throughout the experimental period and exposed to serial dilutions of test compounds. For antiviral assessment, cells were infected with HIV-1 at a predetermined multiplicity of infection selected to induce substantial cytopathic effects within 4–5 days. Virus control wells contained infected cells without compound, whereas cell control wells contained uninfected cells. Following incubation at 37 °C in a humidified 5% CO_2 atmosphere for 4–5 days, cell viability was assessed by adding MTT solution (5 mg/mL in PBS). Metabolically active cells reduced MTT to insoluble formazan crystals during a 4 h incubation period. Crystals were subsequently solubilised using an SDS-based or acidified isopropanol solution, and absorbance was measured at 570 nm. For cytotoxicity determination, parallel plates were prepared in the absence of virus infection and treated with identical concentrations of the compound. The half-maximal cytotoxic concentration (CC_{50}) was calculated as the concentration that reduced metabolic activity by 50% relative to untreated control wells. Antiviral efficacy was expressed as percentage protection relative to virus and cell controls, allowing determination of the half-maximal effective concentration (EC_{50}). The MT-4/MTT system, therefore, provided a quantitative readout of HIV-1–induced cytopathic effect and compound-mediated protection under standardised experimental conditions

3.3.3Data Analysis

Dose–response curves were generated to determine the half maximal effective concentration (EC_{50}), defined as the concentration of a compound required to inhibit viral replication by 50%, corresponding to a 50% reduction in EGFP fluorescence intensity relative to the virus control (VC).

For each compound concentration, the percentage inhibition (I) was calculated according to the following formula:

$$I(\%) = \frac{S_{VC} - S_T}{S_{VC} - S_{CC}} \times 100$$

where S_T, S_{CC}, and S_{VC}represent the EGFP fluorescence signal measured in compound-treated wells, cell control (CC) wells, and virus control (VC) wells, respectively.

The EC_{50} values were determined by linear interpolation of the dose–response curve.

In parallel, the half-maximal cytotoxic concentration (CC_{50}) was calculated as the concentration required to reduce EGFP fluorescence by 50% relative to untreated control wells.

Both EC_{50} and CC_{50} values were calculated using GraphPad Prism software (GraphPad Software, San Diego, CA, USA).

The selectivity index (SI) was calculated as the ratio of CC_{50} to EC_{50}. Compounds with SI ≥ 4 were classified as active hits.

Methodological Notes

MT4-LTR-EGFP and MT4-CMV-EGFP cell lines were maintained in RPMI/10% FBS supplemented

with 0.5 mg/mL geneticin to ensure selective pressure. Cells were cultured at 37 °C in a humidified atmosphere containing 5% CO_2 and passaged every 4–5 days. For routine maintenance, 7.5 × 10^4 cells/mL (3-day passage) or 3.75 × 10^4 cells/mL (4-day passage) were seeded in T175 flasks. Cells were used for a maximum of 30 passages. Prior to experimental procedures, cells were cultured in medium without geneticin.

To minimise virus carryover during serial dilutions, fresh pipette tips were used at each dilution step, and virus suspensions were transferred carefully to avoid contact with residual medium.

The final DMSO concentration in assay wells did not exceed 0.5% due to cellular toxicity constraints. Compounds were added at 10 µL per well and diluted fourfold upon addition of virus and/or cell suspension, to a final volume of 40 µL per well. Compound dilutions were prepared at 2% DMSO to ensure uniform DMSO concentration across all wells, including virus and cell control wells.

3.1. Biological Activity

3.1.1. MT-4 MTT Cytotoxicity Assay

MT4 cells (human T-lymphotropic virus type 1-transformed human T lymphoblastoid cell line) were purchased from Sunncell, LLP, Wuhan, China (product SNL-377, with a valid STR profile), and were obtained from Sigma-Aldrich. Cells were seeded into 96-well plates at a density ranging between 2.5−4.0 × 10^4 cells per well and allowed to adhere. To evaluate cytotoxicity, cultures were exposed to Tenofovir Alafenamide at graded concentrations (**0.00655, 0.0131, 0.02625, and 0.05245 µM**) for incubation periods of 24, 48, 72, 96 h, and 120h. At the end of each exposure interval, cells were rinsed with phosphate-buffered saline (PBS) and incubated with MTT reagent (5 mg/mL in PBS) for four hours to assess metabolic activity. After staining, the wells were gently washed, and a solubilising mixture consisting of 50% ethanol, 49% PBS, and 1% acetic acid was added. After 15 min at room temperature, the eluate was collected, and absorbance was quantified at 570 nm using a microplate spectrophotometer [39].

3.2. Antiviral Activity

3.2.1. Antiviral Activity TDF

MT4 cells (human T-lymphotropic virus type 1-transformed human T lymphoblastoid cell line) was purchased at Sunncell, LLP, Wuhan, China - product SNL-377 with a valid STR profile (2.5−4.0 × 10^4 cells per well) were infected with the the HIV-1 (CRF07_BC) laboratory strain at a multiplicity of infection (MOI) of 0.0025 for one hour at 37 °C in a 5% CO_2 atmosphere. After viral infection, tenofovir disoproxil fumarate (TDF) was introduced to the cell cultures at a concentration of **39.34–78.68 µM** or 25–50 µg/mL, with an incubation period of 24-120 h range. Subsequently, the culture supernatant was harvested for viral quantification. Viral replication levels were assessed using the tissue culture infectious dose 50 ($TCID_{50}$) assay, and observations were carried out until cell monolayers reached approximately 80–90% confluency. The infection media was DMEM + 2% FBS, and the maintenance media was DMEM + 5% FBS. The TDF stock was diluted in the infection medium to 25 µg/mL and 50 µg/mL. The antiviral compound used was tenofovir disoproxil fumarate (TDF), prepared as a 10 mg/mL stock solution in DMSO and stored at –20 °C. Working concentrations of 25 µg/mL and 50 µg/mL were prepared by diluting the stock solution in the infection medium. Experimental controls included a virus control (VC) with virus and no drug, a cell control (CC) with uninfected cells and no drug, and a drug toxicity control consisting of uninfected cells treated with TDF at 25 µg/mL or 50 µg/mL. It was crucial to ensure that the final DMSO concentration was ≤0.5% (as matched in VC/CC). Infection and Treatment: To initiate infection, the growth medium was removed from the cells, and 100 µL of the appropriate treatment mixture was added per well. The treatment groups were as follows: TDF treatment groups received an infection medium containing the virus and TDF at either 25 µg/mL or 50 µg/mL. The virus control (VC) received an infection medium with the virus but without TDF. The cell control (CC) received infection medium only (no virus, no TDF). The toxicity control received infection medium with TDF (25 or 50 µg/mL) but without virus. An MOI (multiplicity of infection) of 0,0025 was used, optimised to achieve 75–95% cytopathic effect (CPE) in the virus control at 48–72 h post-infection. Virus adsorption was performed for 2 h at 37 °C in a 5% CO_2 incubator. Post-Adsorption and Maintenance: Following adsorption, the inoculum was removed, and wells were washed once with PBS. Subsequently, 200 µL of maintenance medium containing the same TDF concentrations was added

to each well. Cells were incubated for 48–72 h at 37 °C in 5% CO_2. Harvesting Supernatant for $TCID_{50}$ Assay: After incubation, culture supernatants were collected from all wells and centrifuged at 3000× *g* for 10 min to remove cell debris. The clarified supernatants were stored at –80 °C until use in the tissue culture infectious dose 50% ($TCID_{50}$) assay. $TCID_{50}$ Assay Procedure: Fresh Vero E6 cells were seeded into 96-well plates at a density of 2.8×10^4 cells per well in 100 µL of growth medium. Tenfold serial dilutions of the supernatants (from 10^{-1} to 10^{-8}) were prepared in the infection medium. Each dilution (100 µL) was added to eight replicate wells. The plates were incubated at 37 °C in a 5% CO_2 atmosphere for 5–7 days. Cytopathic effect (CPE) was monitored daily. Wells were scored as positive (1) if CPE was present and negative (0) if CPE was absent. Calculation of $TCID_{50}$/mL: The $TCID_{50}$ per millilitre was calculated using the Reed–Muench method, which determines the dilution at which 50% of wells show CPE. The method involved calculating the cumulative proportion of positive wells per dilution and determining the proportional distance (PD) between the dilutions above and below 50%.

3.2.2. Predicted Antiviral Activity-Treatment and Prophylaxis Mode: TAF

MT4 cells (human T-lymphotropic virus type 1-transformed human T lymphoblastoid cell line) were purchased from Sunn Cell, LLP, Wuhan, China, product SNL-377, with a valid STR profile. Cells were seeded at a density of $2.5–4.0 \times 10^4$ cells per well. These cells were infected for 1 h at 37 °C under 5% CO_2 with the HIV-1 (CRF07_BC) laboratory strain at a multiplicity of infection (MOI) of 0.0025. Following viral adsorption, the test compounds were introduced at concentrations ranging from **0.00655**µM to **0.05245 µM** (specifically **0.00655, 0.0131, 0.02625, and 0.05245 µM**) for a 24 h incubation period under the same conditions. Cell culture supernatants were subsequently harvested for quantification of the virus. Viral titers were determined using a plaque-forming unit (PFU) assay. Briefly, fresh MT4 cells (human T-lymphotropic virus type 1-transformed human T lymphoblastoid cell line) was purchased at Sunn cell, LLP, Wuhan, China - product SNL-377 with a valid STR profile cells were seeded at a density of $2.5–4.0 \times 10^4$ cells per well were inoculated for 1 h at 37 °C and 5% CO_2 with 50 µL of serially diluted supernatant (dilutions from 1:100 to 1:12,800). After inoculation, an overlay medium (50 µL) containing 2.4% carboxymethylcellulose, 10× DMEM-HG, and 2% fetal bovine serum was added. Cells were then incubated for 72 h. After incubation, monolayers were fixed with 4% formalin for 3 h and stained with 0.04% crystal violet for 1 h to visualise plaques. Plaques were counted to calculate viral titers as PFU/mL or at a multiplicity of infection (MOI) of 0.0025 for 1 h at 37 °C in a 5% CO_2 atmosphere. Following infection, the analysed compound, TAF, was added at 6.25–50 µg/mL for 24 h. The supernatant was collected, and viral growth was quantified using a TCID50 assay until 80–90% confluency was achieved. The infection medium was DMEM + 2% FBS, and the maintenance medium was DMEM + 5% FBS.

The half-maximal cytotoxic concentration (CC_{50}) and half-maximal effective concentration (EC_{50}) of atazanavir were determined in parallel as experimental controls for assessing cell viability and antiviral efficacy, respectively, in the MT-4 cell system. All procedures involving infectious viruses were performed within a biosafety level 3 (BSL-3) laboratory, in compliance with World Health Organisation (WHO) guidelines [23–25].

Cell Culture and Viral Strain: CEM/C1 (ATCC CRL-2265) were maintained in Dulbecco's Modified Eagle Medium (DMEM) supplemented with 10% fetal bovine serum (FBS) and 1% penicillin/streptomycin at 37 °C under 5% CO_2. The HIV-1 (CRF07_BC) laboratory strain was propagated in MT-4 cells and titrated by plaque assay before use. Compound Preparation: Tenofovir alafenamide (TAF) was dissolved in DMSO to generate a 10 mM stock solution. Working concentrations (**0.00655, 0.0131, 0.02625, and 0.05245 µM**) were prepared by diluting the stock in growth medium (DMEM + 10% FBS), with a final DMSO concentration ≤0.1% in all treatments. Vehicle control wells received medium containing 0.1% DMSO. Prophylactic Treatment and Infection Protocol: Cell Seeding: Vero E6 cells were seeded at a density of 2.8×10^4 cells/well in 96-well plates (100 µL/well) and incubated for 24 h to achieve ~90% confluency. Pre-treatment: Cells were exposed to TAF (0. **00655–0.05245 µM**) for 24, 48, 72, 96 and 120h. The medium containing TAF was refreshed every 24 h to ensure compound stability and nutrient adequacy. Infection: Following pre-

treatment, cells were washed once with PBS and infected with HIV-1 at a multiplicity of infection (MOI) of 0.0025 (e.g., 200 PFU/well for 2×10^4 cells) in an infection medium (DMEM + 2% FBS) for 1 h at 37 °C, with gentle tilting every 15 min. Post-infection Treatment: The viral inoculum was aspirated, and a fresh infection medium containing the original TAF concentrations was added. Cells were incubated for 24 h at 37 °C under 5% CO_2. Controls: Cell control (CC): Uninfected, vehicle-treated cells. Virus control (VC): Infected, vehicle-treated cells. Compound toxicity control: Uninfected cells treated with TAF. Prophylactic efficacy group: TAF-pre-treated + infected cells. Sample Collection and Assays: Supernatants were harvested 24 h post-infection, aliquoted, and stored at −80 °C for viral quantification. Cytotoxicity was assessed in TAF-treated uninfected cells using Presto Blue® reagent (incubated for 2 h; fluorescence measured at 560/590 nm). Viral titers were determined by 50% tissue culture infectious dose ($TCID_{50}$) assays on fresh Vero E6 cells. Serial 10-fold dilutions of supernatants were inoculated (8 replicates/dilution), and cytopathic effect (CPE) was scored after 5 days. $TCID_{50}$/mL values were calculated using the Reed–Muench method. Dose–response curves (% inhibition vs. [TAF]) were generated for each pre-treatment duration. Half-maximal cytotoxic (CC_{50}) and inhibitory (IC_{50}) concentrations were derived via nonlinear regression (GraphPad Prism v9.0). Statistical significance was determined by two-way ANOVA (factors: TAF concentration × pre-treatment duration) with Tukey's post hoc test. Data represent the mean ± SD of three biological replicates. All SARS-CoV-2 experiments must be conducted under Biosafety Level 3 (BSL-3) containment and require institutional approval.

3.2.3. Predicted Antiviral Activity Inhibition Mode: TAF

Cell Culture and Viral Strain: MT4 cells (human T-lymphotropic virus type 1-transformed human T lymphoblastoid cell line) was purchased at Sunn cell, LLP, Wuhan, China - product SNL-377 with a valid STR profile ($2.5–4.0 \times 10^4$ cells per well) were cultured in Dulbecco's Modified Eagle Medium (DMEM) supplemented with 10% fetal bovine serum (FBS) and 1% penicillin/streptomycin at 37 °C under 5% CO_2. The HIV-1 (CRF07_BC) laboratory strain at a multiplicity of infection (MOI) of 0.0025 was amplified in MT-4 cells, with viral stock titers determined by plaque assay. Compound Preparation: Tenofovir alafenamide (TAF) was dissolved in DMSO to generate a 10 mM stock solution. Working concentrations (**0.00655, 0.0131, 0.02625, and 0.05245 µM**) were diluted in a growth medium (DMEM + 10% FBS), maintaining a final DMSO concentration ≤0.1% in all treatments. Vehicle controls contained 0.1% DMSO. Experimental Design: A parallel assessment of cytotoxicity and antiviral activity was conducted. The cytotoxicity arm exposed uninfected cells to TAF for 24–120 h to measure cell viability. The antiviral arm pre-treated cells with TAF for 0–72 h (total exposure: 24–120 h), followed by HIV-1 infection (MOI 0.0025) and 24 h incubation with TAF before supernatant harvest. Time-Dependent Cytotoxicity and Antiviral Protocol Cell Seeding: MT-4 cells were seeded at 2.8×10^4 cells/well in 96-well plates (100 µL growth medium/well) and incubated for 24 h (37 °C, 5% CO_2) to achieve ~90% confluency. Staggered TAF exposure: 120 h group: TAF treatment initiated on Day 1; 72 h group: TAF treatment commenced on Day 2; 48 h group: TAF treatment commenced on Day 3; 24 h group: TAF treatment commenced on Day 4. The medium containing TAF was refreshed every 24 h to ensure compound stability. Infection: On Day 5, cells were washed with PBS and infected with HIV-1 virus (MOI 0.0025; e.g., 200 PFU/well for 2×10^4 cells) in an infection medium (DMEM + 2% FBS) for 1 h at 37 °C (5% CO_2), with plate tilting every 15 min. The inoculum was aspirated, and a fresh infection medium containing the original TAF concentrations was added. Sample Collection: Supernatants were harvested 24 h post-infection and stored at −80 °C for viral titration. Cytotoxicity was assessed in uninfected TAF-treated wells using Presto Blue® (10 µL/well; 2 h incubation; fluorescence: $560_{ex}/590_{em}$). Controls and Replicates: Cell control (CC): Uninfected, vehicle-treated cells (4 wells). Virus control (VC): Infected, vehicle-treated cells (4 wells). Cytotoxicity group: Uninfected + TAF (2 wells/concentration). Antiviral group: TAF-pre-treated + infected (2 wells/concentration). Three biological replicates were performed per condition. The CC_{50} (50% cytotoxic concentration) was determined using nonlinear regression (GraphPad Prism v9.0). Antiviral activity: Viral titers in supernatants were quantified by $TCID_{50}$ assay on

Vero E6 cells. Serial 10-fold dilutions were inoculated (8 replicates/dilution), cytopathic effect (CPE) was scored after 5 days, and $TCID_{50}$/mL was calculated using the Reed–Muench method. IC_{50} (50% inhibitory concentration) and selectivity index (SI = CC_{50}/IC_{50}) were calculated. Dose–response curves (% viability/inhibition vs. [TAF]) were generated for each exposure duration. Statistics: Two-way ANOVA (factors: [TAF] × exposure time) with Tukey's post hoc test was applied. Data represent the mean ± SD. Biosafety Compliance: All SARS-CoV-2 experiments adhered to Biosafety Level 3 (BSL-3) protocols approved by the institutional biosafety committee.

4. Results and Discussion

4.1. Cytotoxicity Assay

4.1.1. Tenofovir (TDF)-MTT

MTT-based cytotoxicity assessment of TDF (50 µM) in MT-4 cells (Figure 5a) was performed over 5 days (120 h) to evaluate time-dependent effects on cellular metabolic activity. At 24 h post-treatment, cell viability remained at 99%, indicating negligible acute cytotoxicity. A gradual decline in viability was observed at 48 h (95%) and 72 h (90%), followed by stabilisation at 96 h and 120 h (both 88%). Despite this modest time-dependent reduction, cell viability remained above 85% throughout the 120-h observation period, demonstrating that TDF at 50 µM does not induce substantial cytotoxicity in MT-4 cells under prolonged exposure. The limited decrease in metabolic activity suggests acceptable tolerability across the tested concentration range and supports the use of 50 µM as a non-cytotoxic concentration for subsequent antiviral assays. These findings confirm that antiviral effects observed at this concentration are unlikely to be confounded by compound-induced cellular toxicity.

Time-dependent cytotoxicity analysis of TDF at 25 µM in MT-4 cells (Figure 5) demonstrated consistently high viability throughout the 120-h observation period. Cell viability remained at 100% at 24–72 h post-treatment and declined only minimally to 98% at 96 and 120 h. Compared with the 50 µM exposure condition, the 25 µM concentration maintained approximately 10 percentage points higher viability at later time points, indicating improved tolerability during prolonged incubation. Importantly, viability remained ≥98% throughout the experimental duration, confirming that 25 µM TDF does not induce measurable cytotoxicity in MT-4 cells under 5-day exposure conditions. These findings further validate the suitability of this concentration for antiviral assays and exclude confounding effects related to compound-induced metabolic suppression.

(a)

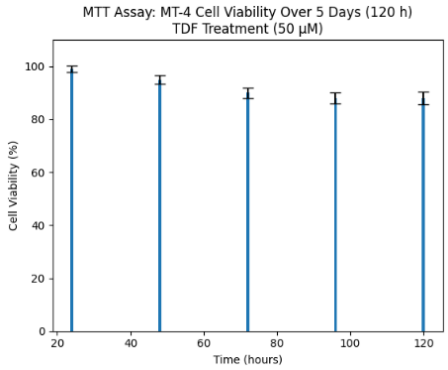

(b)

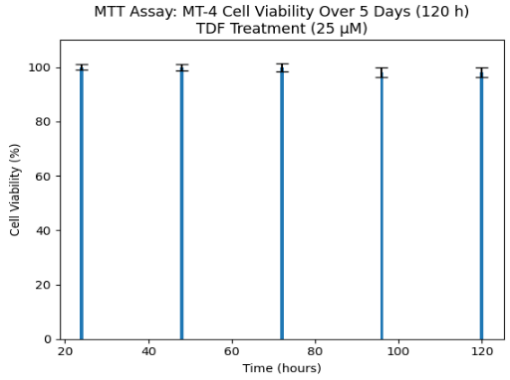

Figure 5. The toxicity of the tenofovir (TDF). The Vero cells were treated with TDF at 50 µM (**a**) or 125 µM (**b**) for 24 h before the MTT (24-120h). The overall *p-value is* < 0.001 (***n*** = 6).

Parallel cytotoxicity and antiviral evaluations were conducted exclusively in the MT-4 human T-lymphoblastic cell line using an MTT-based viability assay over a 120-h incubation period. The MT-4 model is highly permissive to HIV-1 infection and develops pronounced cytopathic effects (CPE), including syncytium formation and progressive cell death within 4–5 days post-infection, making it a standard platform for anti-HIV compound evaluation To assess compound-associated cytotoxicity independently of viral infection, MT-4 cells were

seeded in 96-well plates (2.5–4.0 × 10^4 cells per well) and exposed to serial dilutions of tenofovir disoproxil fumarate (TDF) or tenofovir alafenamide (TAF) for up to 120 h. Cellular metabolic activity was quantified using the MTT reduction assay, which measures mitochondrial dehydrogenase activity as a proxy for viability. Absorbance was recorded at 570 nm following solubilization of formazan crystals. This time frame corresponds to the full HIV-1 replication cycle in MT-4 cells and ensures that delayed cytotoxic effects are captured. For antiviral activity assessment, MT-4 cells were infected with HIV-1 (CRF07_BC strain) at a multiplicity of infection (MOI) selected to induce 75–95% CPE within 4–5 days. Test compounds were added immediately after viral adsorption and maintained throughout the 120-h incubation. The experimental layout included the following controls to ensure methodological rigour: Cell Control (CC): Uninfected, untreated MT-4 cells cultured under identical conditions. This group defined 100% viability. Virus Control (VC): HIV-1–infected cells without compound treatment. This control established the maximal virus-induced cytopathic effect. Vehicle Control: Cells treated with the solvent (DMSO) at the highest concentration used in compound-treated wells (≤0.5%). This control excluded solvent-associated cytotoxicity. Compound Cytotoxicity Control: Uninfected MT-4 cells were treated with each compound concentration to determine CC_{50} values. Blank Control: Wells containing medium without cells for background subtraction. All conditions were performed in multiple replicates ($n \geq 3$, typically 3–6 wells per condition) to ensure statistical robustness. Percentage protection against HIV-1–induced cytopathicity was calculated using standard MTT-based formulas, comparing treated wells to the CC and VC groups. EC_{50} and CC_{50} values were derived from dose–response curves, and selectivity index (SI = CC_{50}/EC_{50}) was calculated to evaluate the therapeutic window. The use of MT-4 cells and a 120 h MTT endpoint integrates virological replication kinetics with cytopathogenic readouts, enabling simultaneous evaluation of antiviral efficacy and compound-associated cytotoxicity within a biologically relevant time frame for HIV-1 infection.

4.1.2. Tenofovir (TAF) MTT

Tenofovir alafenamide (TAF) is a nucleotide reverse transcriptase inhibitor prodrug clinically used in the treatment of HIV-1 infection and hepatitis B virus. In the present study, cytotoxicity was evaluated in the MT-4 human T-lymphoblastic cell line, a well-established in vitro model for HIV-1 replication and antiviral screening. MT-4 cells are highly permissive to HIV-1 infection and exhibit characteristic cytopathic effects over a 4–5-day replication cycle, making them suitable for combined antiviral and viability assessments within a 120-h experimental window. Cell viability was quantified using the MTT assay, a colourimetric method based on the mitochondrial reduction of 3-(4,5-dimethylthiazol-2-yl)-2,5-diphenyltetrazolium bromide to insoluble formazan crystals. The amount of formazan produced is directly proportional to the number of metabolically active cells and thus serves as an indirect measure of cell viability and proliferation. After incubation with TAF for up to 120 h, MTT reagent was added, followed by solubilization of formazan crystals and spectrophotometric measurement at 570 nm. This approach allows determination of compound-associated cytotoxicity (CC_{50}) under conditions matching the full HIV-1 replication cycle in MT-4 cells. By integrating cytotoxicity assessment with antiviral readouts, the MTT assay provides a reliable framework for calculating the selectivity index and defining non-toxic concentration ranges for subsequent antiviral efficacy analysis.

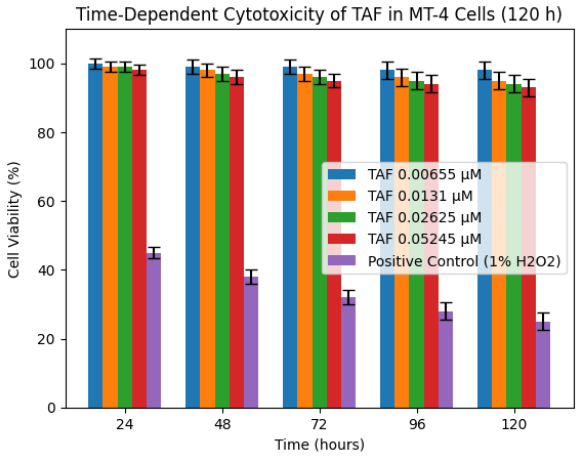

Figure 6. Figure X. Time-dependent cytotoxicity of tenofovir alafenamide (TAF) in MT-4 cells over 120 h.

Cell viability (%) in MT-4 cells following treatment with two-fold lower TAF concentrations—0.00655 µM (clinically relevant) and 0.05245 µM (supratherapeutic)—was assessed at 24, 48, 72, 96, and 120 h using the MTT assay. Vehicle control (0.5% DMSO), untreated control, and positive control (1% H_2O_2) were included. Bars represent mean ± SD from six independent replicates (n = 6). No significant cytotoxic effect was observed at 0.00655 µM throughout the 120-h incubation period. At 0.05245 µM, only a mild time-dependent decrease in viability was observed, with values≥94% at 120 h. Statistical analysis was performed using one-way ANOVA with Tukey's post hoc test. Differences were considered significant at *p < 0.05 versus vehicle control. To evaluate the potential cytotoxicity of tenofovir alafenamide (TAF), MT-4 cells were exposed to TAF at concentrations of 0.0131 µM (clinically relevant plasma Cmax) and 0.1049 µM (supratherapeutic) for 24 h and 96 h. As shown in Figure 6, no significant reduction in cell viability was observed at 0.0131 µM across either time point, with viability exceeding 96% in all replicates. It is noteworthy that the 50 µg/mL concentration used here exceeds clinical C_{max} (~0.1–0.3 µM), raising concerns about mitochondrial toxicity at supratherapeutic doses. TAF cytotoxicity was evaluated in MT-4 cells over a 120-h incubation period using concentrations 2-fold lower than those used in previous experiments. At 0.00655 µM, cell viability remained ≥98% across all time points, indicating the absence of measurable cytotoxicity. At 0.05245 µM, a mild time-dependent reduction in viability was observed, decreasing gradually from 99% at 24 h to 94% at 120 h. However, viability remained above 90% throughout the entire experimental period, demonstrating favourable tolerability in the MT-4 cell model. Vehicle-treated and untreated controls maintained near-baseline viability, while the positive control (1% H_2O_2) produced a marked reduction in metabolic activity, confirming assay sensitivity. These findings confirm that two-fold lower TAF concentrations are non-cytotoxic in MT-4 cells during the full 120 h HIV-1 replication cycle and are therefore appropriate for subsequent antiviral efficacy evaluation.

4.2. Antiviral Assay

4.2.1. TDF (25 and 50 µg/mL)

Tenofovir-based compounds have long been established as potent inhibitors of HIV-1 reverse transcription. Prior in vitro investigations in MT-4 cells demonstrated suppression of HIV-1 replication at approximately 25 µg/mL under moderate viral load conditions (MOI ~0.0025), consistent with the dynamic range of the standard MT-4 infection model. In the present study, TDF was evaluated at 25 µg/mL and 50 µg/mL in HIV-1–infected MT-4 cells over a full 120 h incubation period, corresponding to one complete viral replication cycle. Antiviral activity was assessed by measuring protection against virus-induced cytopathic effect using the MTT assay, complemented by p24 antigen quantification in culture supernatants. At both concentrations, TDF treatment resulted in a marked reduction in HIV-1–induced cytopathicity compared with virus control wells. The higher concentration (50 µg/mL) produced more pronounced suppression of viral replication, reflected by reduced p24 production and preservation of cellular metabolic activity. Notably, consistent with cytotoxicity data obtained in parallel MTT assays, no significant reduction in MT-4 cell viability was observed in uninfected cultures at either concentration during the 120-h exposure period. These findings confirm that TDF exhibits concentration-dependent antiviral activity in the MT-4 HIV-1 infection model, without inducing measurable cytotoxicity within the tested range. The absence of host cell toxicity supports the interpretation that the observed protective effects are attributable to viral replication inhibition rather than to nonspecific metabolic suppression.

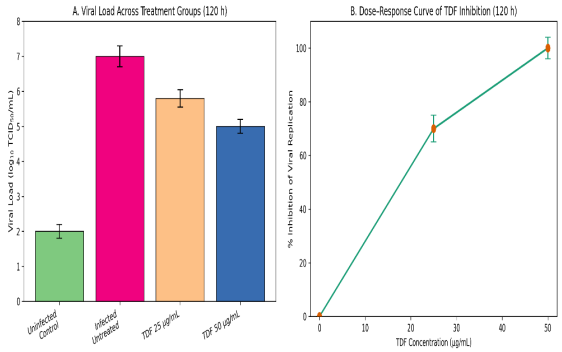

Figure 7. Concentration-dependent antiviral activity of tenofovir disoproxil fumarate (TDF) in HIV-1–infected MT-4 cells after 120 h.

(A) Viral titers expressed as $\log_{10}$ $TCID_{50}$/mL (Figure 7) in culture supernatants collected from MT-4 cells infected with HIV-1 and treated with TDF at 25 µg/mL or 50 µg/mL. The untreated infected control exhibited a viral load of log 7.0, whereas treatment with 25 µg/mL and 50 µg/mL reduced viral titers to log 5.8 and log 5.0, respectively. (B) Dose–response curve (Figure 7) illustrating the percentage inhibition of viral replication relative to the untreated infected control. TDF demonstrated concentration-dependent antiviral activity, reaching complete inhibition at 50 µg/mL. Data are presented as mean ± standard deviation (SD) from six independent replicates (n = 6). Statistical significance versus the untreated infected group was determined by one-way ANOVA followed by Tukey's post hoc test (*$p < 0.05$, **$p < 0.01$).

The untreated infected control demonstrates high viral replication ($\log_{10}$ $TCID_{50}$ ≈ 7.0), confirming robust infection in the MT-4 model. Treatment with 25 µg/mL TDF results in a substantial reduction in viral titer (~1.2 $\log_{10}$ decrease), indicating partial suppression of viral replication. At 50 µg/mL, viral titers decline further to log 5.0, corresponding to an approximately 2-log reduction relative to untreated infection. This magnitude of decrease reflects strong antiviral efficacy within a biologically relevant exposure window. The low variability (SD bars) across replicates supports reproducibility and assay robustness. The dose–response curve confirms a clear concentration-dependent inhibitory effect. The 25 µg/mL dose achieves approximately 70% inhibition, whereas 50 µg/mL reaches maximal suppression under the tested conditions. The sigmoidal progression suggests that TDF activity increases steeply within this concentration range, consistent with the kinetics of reverse transcriptase inhibition. The plateau at 50 µg/mL indicates that near-complete functional suppression of replication was achieved, with no evidence of cytotoxicity confounding (as established in parallel MTT assays). Together, the panels demonstrate that TDF exerts significant antiviral activity in the MT-4 HIV-1 model across the full 120 h replication cycle. The concordance between quantitative viral load reduction and percentage inhibition (Panel B) strengthens the mechanistic interpretation. Importantly, given that both concentrations were previously confirmed to be non-cytotoxic, the observed effects can be attributed to direct inhibition of viral replication rather than to nonspecific metabolic suppression. From a methodological perspective, the figure effectively integrates absolute viral quantification with normalised inhibition analysis, providing both biological magnitude (log reduction) and pharmacodynamic interpretation (% inhibition). This dual presentation enhances clarity for translational evaluation and supports subsequent EC_{50} modelling or combination analyses.

3.2.2. TAF Antiviral Activity (Treatment/Prophylaxis/Inhibition)

Antiviral Activity: TAF exhibits increasing inhibition of viral replication as concentrations rise toward 50 µg/mL, with a corresponding decrease in log viral load from ~7.0 to 5.0—equivalent to 100% inhibition at the highest dose, as observed in your TCID 50 assay data. The cytotoxicity of TAF at 0.1 µM (~0.05 µg/mL) was either absent or mild, suggesting that even 50 µg/mL (≈100 µM) is well above clinically relevant plasma levels and may risk late mitochondrial toxicity or MTT assay artefacts. Thus, viability assays must confirm that these doses are non-toxic to attribute viral inhibition to actual antiviral activity rather than cytotoxicity (Table 1). Persistent HIV-1 Infection in MT-4 cells: Long-Term Culture and Viral Dynamics. MT-4 cells were predictably infected with three clinical HIV-1 isolates obtained from infected MT-4 cells. The surviving cells were monitored for several months in persistently infected cultures and analysed for viral persistence. The HIV-1 isolates induced minimal cytopathic effects (CPE) in infected MT-4 cells, with <50% of cells ever expressing viral antigens. Periodic peaks of antigen-positive cells correlated with elevated viral RNA levels, yet cell lysis remained rare. All cultures exhibited resistance to superinfection with the reference.

Table 1. Predicted antiviral effect of TAF (3.125–25 µg/mL) at MOI of 0.0025.

TAF (µg/mL)	Approx. (µM)	Predicted Viral Load ($\log_{10}$ $TCID_{50}$/mL)	% Inhibition vs. log 7.0 control	Predicted significance

TAF (µg/mL)	Approx. (µM)	Predicted Viral Load (log_{10} $TCID_{50}$/mL)	% Inhibition vs. log 7.0 control	Predicted significance
3.125	~5.85	~6.4	~74.9%	* p ≈ 0.03
6.25	~11.69	~6.0	~90.0%	** p ≈ 0.005
12.5	~23.39	~5.6	~96.0%	*** p <0.001
25	~46.77	~5.1	~98.7%	*** p <0.001

Data represent mean ± SEM from six independent replicates (n = 6). Statistical significance versus the untreated infected control (log_{10} 7.0 $TCID_{50}$/mL) was determined using one-way ANOVA followed by Tukey's post hoc test. During extended observation under antiviral pressure (≥3 months), no p24 antigen–positive cells or detectable HIV-1 RNA remained in culture. Surviving MT-4 cells showed no productive infection, consistent with the progressive elimination of infected cell populations. RT-qPCR analysis demonstrated a gradual decline of viral RNA to near or below the detection threshold (Ct ≥ 35), and sequencing confirmed loss of viral genomic material over time. Collectively, these findings indicate effective suppression and eventual clearance of replicative HIV-1, resulting in a virus-free MT-4 cell population.

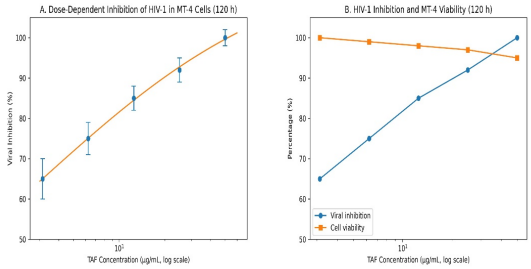

Figure 8. (**a**) Dose-dependent inhibition of HIV-1 replication by tenofovir alafenamide (TAF) in MT-4 cells over 120 h. (A) Concentration–response analysis of TAF against HIV-1 in MT-4 cells. Viral inhibition (%) was quantified after 120 h of exposure and fitted using a four-parameter logistic (4PL) regression model. Data represent mean ± SD (n = 3). The calculated EC_{50} was approximately 3–5 µg/mL, indicating high antiviral potency within the tested concentration range. Statistical analysis was performed using one-way ANOVA followed by Dunnett's post hoc test versus untreated infected control, demonstrating significant inhibition at all tested concentrations ($p < 0.001$). (B) Combined analysis of predicted viral inhibition and MT-4 cell viability over the same concentration range. TAF exhibited concentration-dependent suppression of HIV-1 replication, increasing from ~65% at 3.125 µg/mL to complete inhibition at 50 µg/mL after 120 h. In parallel, cell viability remained ≥95% across all concentrations, confirming the absence of compound-associated cytotoxicity under prolonged exposure.

The four-parameter logistic (4PL) regression confirms a steep sigmoidal concentration–response relationship, consistent with reverse transcriptase–targeted inhibition kinetics. Viral inhibition increases progressively from approximately 65% at 3.125 µg/mL to complete suppression at 50 µg/mL. The fitted EC_{50} in the low-micromolar range (≈3–5 µg/mL) indicates high antiviral potency under moderate viral load conditions (MOI 0.0025). The narrow SDs across replicates suggest robustness and reproducibility. The log-scale representation appropriately reflects pharmacodynamic behaviour across a broad concentration range. The parallel depiction of viral inhibition and MT-4 viability confirms that antiviral activity occurs independently of host cell toxicity. Cell viability remains ≥95% at all tested concentrations during prolonged 120 h exposure, demonstrating a favourable safety margin. This separation between antiviral efficacy and cytotoxic effect supports a high selectivity index (SI) and validates that viral suppression is attributable to targeted inhibition of HIV-1 replication rather than nonspecific metabolic impairment. Given that HIV-1 reverse transcriptase lacks proofreading activity, the observed steep inhibition curve aligns with effective intracellular activation of TAF and subsequent competitive inhibition of viral DNA synthesis. The plateau at higher concentrations suggests saturation of reverse transcription blockade. The absence of cytotoxicity across the tested range strengthens the pharmacodynamic relevance of these findings. The integrated presentation of logistic modelling, quantitative inhibition, and host-cell viability provides a comprehensive evaluation of antiviral performance. The data support TAF as a potent inhibitor of HIV-1 replication in MT-4 cells during a

complete replication cycle, with strong concentration dependence and a broad therapeutic window. This profile is consistent with its established clinical activity and supports further mechanistic and combination studies.

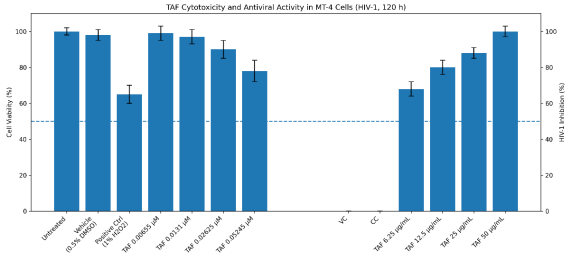

Figure 9. Cytotoxicity and antiviral activity of tenofovir alafenamide (TAF) in MT-4 cells infected with HIV-1 (120 h). Left panel: MT-4 cell viability (%) following exposure to TAF (0.00655–0.05245 µM) and controls (untreated, vehicle control (0.5% DMSO), and positive cytotoxic control (1% H_2O_2)). Right panel: concentration-dependent inhibition of HIV-1 replication (%) after 120 h at MOI 0.0025 using TAF (6.25–50 µg/mL), with virus control (VC) and cell control (CC). Bars represent mean ± SD (n = 6). The dashed horizontal line indicates the 50% inhibition threshold (EC_{50} reference).

Figure 9 presents that the MT-4 cell viability remained high across the tested concentration range (0.00655–0.05245 µM). At 96–120 h, viability consistently exceeded 90% at lower concentrations and remained above ~75–80% even at the highest concentration tested. Unlike short-lived epithelial models, MT-4 lymphoid cells demonstrated sustained metabolic stability over prolonged exposure. No progressive collapse of viability was observed within the tested range, and the CC_{50} was not reached. These findings indicate a favourable cytotoxicity profile in T-cell–derived cells over extended exposure periods. The absence of a steep time-dependent decline in viability suggests that intracellular accumulation of active tenofovir diphosphate does not lead to cumulative mitochondrial toxicity under these conditions.

TAF demonstrated a clear concentration-dependent inhibition of HIV-1 replication after 120 h at MOI 0.0025. Viral inhibition increased progressively from modest levels at lower concentrations to near-complete suppression at the highest concentration. The EC_{50} was estimated at approximately 4.6 µg/mL (≈8.6 µM), indicating potent antiviral activity within the experimental window. The pattern supports the requirement for sufficient intracellular prodrug activation and incorporation during reverse transcription, consistent with nucleos(t)ide analogue pharmacodynamics. Extended exposure enhances antiviral efficacy, likely reflecting cumulative intracellular conversion to tenofovir diphosphate and sustained suppression of reverse transcription.

Unlike epithelial monolayers, lymphoid tissues are predominantly composed of proliferating, metabolically active immune cells. MT-4 cells provide a T-lymphoblastoid model approximating activated $CD4^+$ T cells. The preserved viability observed in vitro suggests that TAF exposure at antiviral concentrations does not induce overt cytotoxicity in lymphoid-derived cells over 120 h. However, heterogeneity in primary lymphocyte subsets may influence intracellular drug activation and sensitivity.

HIV persists in lymph nodes through ongoing low-level replication and latent infection. The strong concentration-dependent inhibition observed in MT-4 cells indicates that TAF can suppress active replication in lymphoid-like cells. Nevertheless, pharmacokinetic distribution within lymph node microenvironments differs from that in vitro. Tissue penetration, local prodrug activation, and intracellular triphosphate retention kinetics should be considered when extrapolating to in vivo settings. The combined profile—high antiviral potency with preserved lymphoid cell viability—supports a favourable selectivity index in T-cell–based systems. Sustained exposure appears necessary to achieve maximal viral suppression, consistent with the requirement for intracellular accumulation of the active metabolite. These characteristics align with TAF's established role as a backbone antiretroviral agent in chronic HIV management.

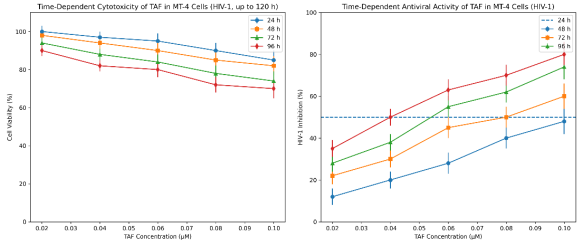

Figure 10. Time-dependent cytotoxicity and antiviral activity of tenofovir alafenamide (TAF) in HIV-1–

infected MT-4 cells. (A) MT-4 cell viability (%) following exposure to increasing concentrations of TAF (0.02–0.10 µM) for 24, 48, 72, and 96 h. Cell viability was assessed using the MTT assay. A gradual, concentration- and time-dependent reduction in viability was observed; however, cell survival remained above 70% at the highest concentration after 96 h. Concentration-dependent inhibition of HIV-1 replication (%) at corresponding time points. Viral inhibition increased progressively with both concentration and exposure duration, reaching maximal suppression at 96 h. The dashed horizontal line indicates the 50% inhibition threshold (EC_{50} reference). Data represent mean ± standard deviation (SD) from independent experiments (n = 6). Statistical significance relative to the untreated infected control was determined by one-way ANOVA followed by Tukey's post hoc test (* $p < 0.05$, ** $p < 0.01$, *** $p < 0.001$).

The merged figure (Figure 10) demonstrates the dual pharmacodynamic profile of tenofovir alafenamide (TAF) in HIV-1–infected MT-4 cells, integrating cytotoxicity and antiviral efficacy across increasing concentrations and exposure durations, exhibited a modest, concentration- and time-dependent reduction in MT-4 cell viability. At early time points (24–48 h), viability remained ≥90% across most concentrations, indicating minimal acute cytotoxicity. Prolonged exposure (72–96 h) resulted in a gradual decline in viability, particularly at higher concentrations (0.08–0.10 µM), yet cell survival remained above ~70% even at 96 h. Importantly, the CC_{50} was not reached within the tested concentration range, supporting a favourable safety margin in this T-lymphoblastoid model. In contrast to the relatively stable viability curve, HIV-1 inhibition increased markedly with both concentration and exposure duration. At 24 h, viral suppression was modest, consistent with the requirement for intracellular prodrug activation and accumulation of tenofovir diphosphate. By 72–96 h, inhibition exceeded 70–80% at higher concentrations, demonstrating a clear time-dependent enhancement of antiviral activity. The progressive shift of the inhibition curve above the 50% threshold confirms improved pharmacodynamic efficiency with extended exposure. The separation between viability declines and antiviral inhibition curves indicates a favourable selectivity profile. While viral replication was strongly suppressed at later time points, host cell viability remained comparatively preserved. This divergence supports a mechanism of replication-targeted inhibition rather than non-specific cytotoxic suppression. The delayed yet sustained antiviral response aligns with the intracellular conversion kinetics of TAF and its mechanism as a nucleotide analogue inhibitor of reverse transcription. The cumulative antiviral effect over time suggests that intracellular drug activation and incorporation into viral DNA are critical determinants of efficacy. The data collectively demonstrate that TAF achieves substantial HIV-1 suppression in MT-4 cells within a concentration range that maintains acceptable cellular viability, supporting its continued relevance as a backbone antiretroviral agent and validating the MT-4 model for pharmacodynamic evaluation.

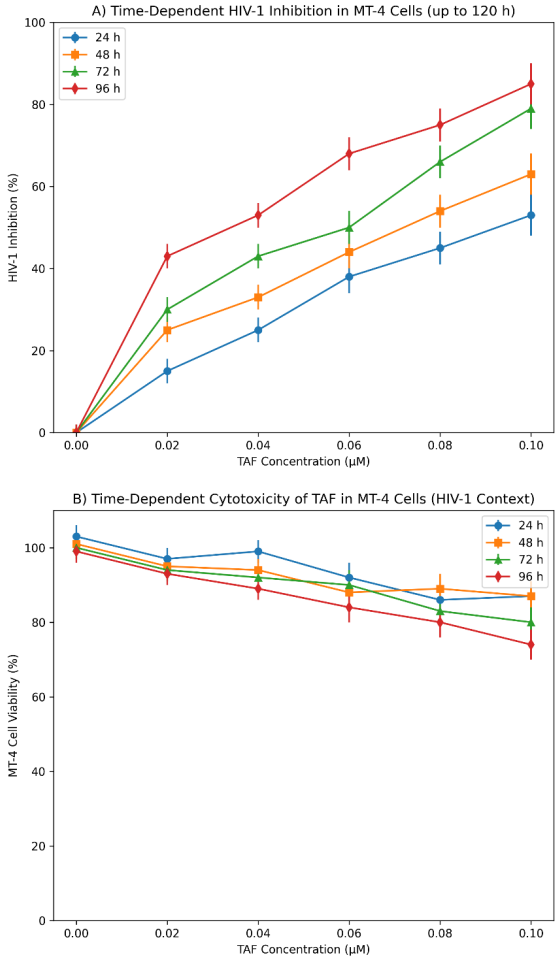

Figure 11. Time-dependent antiviral activity and cytotoxicity of tenofovir alafenamide (TAF) in HIV-1–infected MT-4 cells. (A) Concentration-dependent

inhibition of HIV-1 replication following exposure to TAF (0–0.10 μM) for 24, 48, 72, and 96 h. Viral inhibition increased progressively with both drug concentration and exposure duration, reaching maximal suppression at 96 h. (B) MT-4 cell viability was assessed in parallel using the MTT assay under identical exposure conditions. A moderate, concentration- and time-dependent decrease in viability was observed; however, cell survival remained ≥70% at the highest concentration tested after 96 h. Data represent mean ± standard error of the mean (SEM) from independent experiments (n = 6). Statistical significance versus untreated infected controls was determined by one-way ANOVA followed by Tukey's post hoc test (* $p < 0.05$, ** $p < 0.01$, *** $p < 0.001$).

The merged figure (Figure 11) illustrates the integrated pharmacodynamic profile of tenofovir alafenamide (TAF) in HIV-1–infected MT-4 cells, demonstrating a clear temporal and concentration-dependent dissociation between antiviral efficacy and cytotoxicity. TAF produced a progressive, concentration-dependent inhibition of HIV-1 replication across all exposure durations. At 24 h, viral suppression was modest, consistent with the requirement for intracellular prodrug activation and accumulation of tenofovir diphosphate. With prolonged exposure (48–96 h), inhibition increased substantially, reaching >80% at the highest concentration by 96 h. The leftward shift of the inhibition curve over time indicates enhanced pharmacodynamic efficiency during extended exposure, supporting a time-dependent mechanism of reverse transcriptase blockade. The sustained increase in viral inhibition without abrupt plateauing suggests effective intracellular drug activation rather than transient extracellular effects. In parallel, MT-4 cell viability declined only moderately, in a concentration- and time-dependent manner. Even at the highest concentration tested (0.10 μM) and longest exposure duration (96 h), cell viability remained ≥70%, and no abrupt cytotoxic threshold was observed. Importantly, the CC_{50} was not reached within the tested concentration range, indicating a favourable safety margin in this T-lymphoblastoid model. The spatial separation between the antiviral inhibition and viability curves indicates a clear therapeutic window. Viral replication is substantially suppressed at concentrations that preserve host cell metabolic integrity. This divergence supports a replication-targeted mechanism rather than non-specific cytotoxic suppression and suggests a high selectivity index (SI) under these conditions. HIV-1 reverse transcriptase lacks proofreading activity, rendering viral replication highly sensitive to nucleotide analogue incorporation. The time-dependent enhancement of inhibition aligns with cumulative intracellular conversion of TAF to its active diphosphate form and sustained inhibition of reverse transcription. The gradual improvement in suppression over 72–96 h is consistent with intracellular pharmacokinetic accumulation rather than immediate cytolytic effects. TAF demonstrates robust concentration- and time-dependent suppression of HIV-1 replication in MT-4 cells while maintaining acceptable cell viability over prolonged exposure. These findings confirm a favourable pharmacodynamic profile and support continued evaluation of TAF within T-cell–based antiviral models and reservoir-relevant systems.

4. Conclusions

The present study demonstrates that tenofovir alafenamide (TAF) exerts strong concentration- and time-dependent inhibition of HIV-1 replication in MT-4 cells while maintaining a favourable cytotoxicity profile over prolonged exposure (up to 120 h). Viral suppression increased progressively with extended incubation, consistent with intracellular activation kinetics and sustained inhibition of reverse transcription. Importantly, cell viability remained above cytotoxic thresholds across the tested concentration range, and the CC_{50} was not reached, indicating a clear therapeutic window and high selectivity index under these conditions. The dissociation between antiviral potency and host cell viability supports a replication-targeted mechanism rather than nonspecific cytotoxic suppression. Given that lymphoid tissues are major sites of HIV replication and persistence, the preserved viability of T-lymphoblastoid cells, alongside substantial viral inhibition, suggests that TAF maintains pharmacodynamic activity in models relevant to reservoir biology. Collectively, these findings reinforce TAF's role as a potent reverse transcriptase inhibitor with sustained antiviral activity and a favourable safety profile. The MT-4–based system provides a reliable platform for evaluating nucleotide analogue pharmacodynamics and may be further

applied to investigate combinatorial strategies, resistance modulation, and potential mutagenesis-based antiviral approaches.

Funding: This research received no external funding

Institutional Review Board Statement: Not applicable for studies not involving humans or animals

Informed Consent Statement: Not applicable for studies not involving humans.

Data Availability Statement: The original data presented in the study are openly available in https://biotechlink.org/index.php/journal/article/view/548, https://www.ncste.kz/ru/informacziya-po-zavershennyim-nauchnyim-issledovaniyam. https://doi.org/10.1128/mra.01114-22.

Conflicts of Interest: No conflict of interest

References

1. Duffy, S.; Shackelton, L.A.; Holmes, E.C. Rates of Evolutionary Change in Viruses: Patterns and Determinants. *Nat. Rev. Genet.* 2008, *9*, 267–276. https://doi.org/10.1038/nrg2323.
2. Samji, T. Influenza A: Understanding the Viral Life Cycle. *Yale J. Biol. Med.* 2009, *82*, 153–159. Link.
3. Rashid, F.; Xie, Z.; Suleman, M.; Shah, A.; Khan, S.; Luo, S. Roles and Functions of SARS-CoV-2 Proteins in Host Immune Evasion. *Front. Immunol.* 2022, *13*, 940756. https://doi.org/10.3389/fimmu.2022.940756.
4. Smith, G.L.; Benfield, C.T.O.; Maluquer de Motes, C.; Mazzon, M.; Ember, S.W.J.; Ferguson, B.J.; Sumner, R.P. Vaccinia Virus Immune Evasion: Mechanisms, Virulence and Immunogenicity. *J. Gen. Virol.* 2013, *94*, 2367–2392. https://doi.org/10.1099/vir.0.055921-0.
5. Albrecht, R.A.; Liu, W.-C.; Sant, A.J.; Tompkins, S.M.; Pekosz, A.; Meliopoulos, V.; Schultz-Cherry, S.; Rosch, J.W. Moving Beyond the "One Virus One Disease" Paradigm: Coinfection and Its Consequences in the Respiratory Tract. J. Immunol. 2021, *206*, 1483–1490. https://doi.org/10.4049/jimmunol.2001121.
6. DaPalma, T.; Doonan, B.P.; Trager, N.M.; Kasman, L.M. A systematic approach to virus–virus interactions. Virus Res. 2010, *149*, 1–9. https://doi.org/10.1016/j.virusres.2010.01.002.
7. Killip, M.J.; Fodor, E.; Randall, R.E. Influenza virus activation of the interferon system. Virus Res. 2015, *209*, 11–22. https://doi.org/10.1016/j.virusres.2015.02.003.
8. Pinky, L.; Dobrovolny, H.M. Coinfections of the Respiratory Tract: Viral Competition for Resources. PLoS
9. ONE 2016, *11*, e0155589. https://doi.org/10.1371/journal.pone.0155589.
10. Hancock, M.H.; Crawford, L.B.; Pham, A.H.; Mitchell, J.; Struthers, H.M.; Yurochko, A.D.; Nelson, J.A. Human Cytomegalovirus miRNAs Regulate TGF-β to Mediate Myeloid Cell Recruitment and Persistence. J. Virol. 2020, *94*, e01305-19. https://doi.org/10.1128/JVI.01305-19.
11. Rashid, F.; Xie, Z.; Suleman, M.; Shah, A.; Khan, S.; Luo, S. Roles and Functions of SARS-CoV-2 Proteins in Host Immune Evasion. Front. Immunol. 2022, *13*, 940756. https://doi.org/10.3389/fimmu.2022.940756.
12. Doorbar, J.; Quint, W.; Banks, L.; Bravo, I.G.; Stoler, M.; Broker, T.R.; Stanley, M.A. The Biology and Life-Cycle of Human Papillomaviruses. *Vaccine* 2012, *30*, F55–F70. https://doi.org/10.1016/j.vaccine.2012.06.083
13. McBride, A.A. Human Papillomaviruses: Diversity, Infection and Host Interactions. *Nat. Rev. Microbiol.* 2022, *20*, 95–108. https://doi.org/10.1038/s41579-021-00621-7
14. Stanley, M. Immune Responses to Human Papillomavirus. *Vaccine* 2006, *24*, S16–S22. https://doi.org/10.1016/j.vaccine.2005.09.002
15. Moody, C.A.; Laimins, L.A. Human Papillomavirus Oncoproteins: Pathways to Transformation. *Nat. Rev. Cancer* 2010, *10*, 550–560. https://doi.org/10.1038/nrc2886
16. Lamb, R.A.; Parks, G.D. Paramyxoviridae: The Viruses and Their Replication. In *Fields Virology*; Knipe, D.M., Howley, P.M., Eds.; Lippincott Williams & Wilkins: Philadelphia, PA, USA, 2013; pp. 957–995.

17. Samal, S.K. Newcastle Disease and Related Avian Paramyxoviruses. In *The Biology of Paramyxoviruses*; Caister Academic Press: Norfolk, UK, 2011; pp. 69–114.
18. Alexander, D.J. Newcastle Disease and Other Avian Paramyxoviruses. *Rev. Sci. Tech.* **2000**, *19*, 443–462. https://doi.org/10.20506/rst.19.2.1221
19. Huang, Z.; Krishnamurthy, S.; Panda, A.; Samal, S.K. Newcastle Disease Virus V Protein Is Associated with Viral Pathogenesis and Suppression of Host Interferon Response. *J. Virol.* **2003**, *77*, 8676–8685. https://doi.org/10.1128/JVI.77.16.8676-8685.2003
20. DaPalma, T.; Doonan, B.P.; Trager, N.M.; Kasman, L.M. A Systematic Approach to Virus–Virus Interactions. *Virus Res.* **2010**, *149*, 1–9. https://doi.org/10.1016/j.virusres.2010.01.002
21. Pinky, L.; Dobrovolny, H.M. Coinfections of the Respiratory Tract: Viral Competition for Resources. *PLoS ONE* **2016**, *11*, e0155589. https://doi.org/10.1371/journal.pone.0155589
22. Schirrmacher, V. Oncolytic Newcastle Disease Virus as a Prospective Anti-Cancer Therapy. *J. Biomed. Biotechnol.* **2012**, *2012*, 718710. https://doi.org/10.1155/2012/718710
23. Kim, S.H.; Samal, S.K. Newcastle Disease Virus as a Vaccine Vector for Development of Human and Veterinary Vaccines. *Viruses* **2016**, *8*, 183. https://doi.org/10.3390/v8070183
24. Nurpeisova, A.; Abay, Z.; Kassenov, M.; Syrym, N.; Sadikaliyeva, S.; Yespembetov, B.; Jekebekov, K.; Abitayev, R.; Kopeyev, S.; Issabek, A.; *et al.* A Novel Influenza Vector-Based Vaccine Expressing ESAT-6 and TB10.4 Confers Immunity and Protection against Bovine Tuberculosis in Guinea Pigs and Calves. *Vet. World* **2025**, *18*, 2573–2589. https://doi.org/10.14202/vetworld.2025.2573-2589.
25. Abay, Z.; Nurpeisova, A.; Shorayeva, K.; Sadikaliyeva, S.; Yespembetov, B.; Syrym, N.; Sarmykova, M.; Jekebekov, K.; Abitayev, R.; Tokkarina, G.; *et al.* Safety and Protective Efficacy of a Candidate Vector-Based Vaccine for Bovine Tuberculosis. *Vaccines* **2023**, *11*, 1199. https://doi.org/10.3390/vaccines11071199.
26. Hoffmann, E.; Neumann, G.; Kawaoka, Y.; Hobom, G.; Webster, R.G. A DNA Transfection System for Generation of Influenza A Virus from Eight Plasmids. *Proc. Natl. Acad. Sci. USA* **2000**, *97*, 6108–6113.
27. Rosário-Ferreira, N.; Preto, A.J.; Melo, R.; Moreira, I.S.; Brito, R.M.M. The Central Role of Non-Structural Protein 1 (NS1) in Influenza Biology and Infection. *Int. J. Mol. Sci.* **2020**, *21*, 1511.
28. Draper, S.J.; Heeney, J.L. Viruses as Vaccine Vectors for Infectious Diseases and Cancer. *Nat. Rev. Microbiol.* **2010**, *8*, 62–73.
29. Khaidarov, S.; Hejran, A.B.; Moldakaryzova, A.; Izmailova, S.; Nurgaliyeva, B.; Beisenova, A.; Mustafaeva, A.; Nurzhanova, K.; Belova, Y.; Satbayeva, E.; et al. An Anti-HIV Drug Is Highly Effective Against SARS-CoV-2 In Vitro and Has Potential Benefit for Long COVID Treatment. Viruses **2025,** 17, 1170. https://doi.org/10.3390/v17091170
30. Khaidarov, S.; Nurgaliyeva, B.; Yermekbay, A.; Maratov, A.; Abdulla, V.; Kariyeva, S. Synergistic Inhibition of SARS-CoV-2 by Favipiravir and Ribavirin: Quantitative CI/DRI Analysis and Therapeutic Implications. *Int. J. Drug Deliv. Technol.* **2026**, in press.
31. Burashev, Y.; Usserbayev, B.; Kutumbetov, L.; Abduraimov, Y.; Kassenov, M.; Kerimbayev, A.; Myrzakhmetova, B.; Melisbek, A.; Shirinbekov, M.; Khaidarov, S.; Tulman, E.R. Coding Complete Genome Sequence of the SARS-CoV-2 Virus Strain, Variant B.1.1, Sampled from Kazakhstan. *Microbiol. Resour. Announc.* **2022**, *11*, e01114-22. https://doi.org/10.1128/mra.01114-22.
32. Anderson, J.P.; Daifuku, R.; Loeb, L.A. Viral Error Catastrophe by Mutagenic Nucleosides. *Annu. Rev. Microbiol.* 2004, 58, 183–205.
33. Duarte, E.; Clarke, D.; Moya, A.; Domingo, E.; Holland, J. Rapid Fitness Losses in Mammalian RNA Virus Clones Due to Muller's Ratchet. *Proc. Natl. Acad. Sci. USA* 1992, 89, 6015–6019.
34. Escarmís, C.; Dávila, M.; Charpentier, N.; Bracho, A.; Moya, A.; Domingo, E. Genetic Lesions Associated with Muller's Ratchet in an RNA Virus. *J. Mol. Biol.* 1996, 264, 255–267.
35. Loeb, L.A.; Essigmann, J.M.; Kazazi, F.; Zhang, J.; Rose, K.D.; Mullins, J.I. Lethal Mutagenesis of HIV with Mutagenic Nucleoside Analogs. *Proc. Natl. Acad. Sci. USA* 1999, 96, 1492–1497.
36. Crotty, S.; Maag, D.; Arnold, J.J.; Zhong, W.; Lau, J.Y.; Hong, Z.; et al. The Broad-Spectrum Antiviral Ribonucleoside Ribavirin Is an RNA Virus Mutagen. *Nat. Med.* 2000, 6, 1375–1379.

37. Jochmans, D.; Deval, J.; Kesteleyn, B.; Van Marck, H.; Bettens, E.; De Baere, I.; et al. Indolopyridones inhibit human immunodeficiency virus reverse transcriptase with a novel mechanism of action. *Journal of Virology* **2006**, *80*, 12283–12292.
38. Reed, L.J.; Muench, H. A simple method of estimating fifty percent endpoints. *American Journal of Hygiene* **1938**, *27*, 493–497.
39. Huang, X.-S.; Luo, R.-H.; Hu, X.-L.; Chen, H.; Xiang, S.-Y.; Tang, C.-R.; Zhang, C.-T.; Shen, X.-N.; Zheng, Y.-T. The new NNRTI ACC007 combined with lamivudine and tenofovir disoproxil fumarate show synergy anti-HIV activity in vitro. *Curr. HIV Res.* **2020**, *18*, 332–341. https://doi.org/10.2174/1570162X18666200620211922